Nuclear Magnetic Resonance Fourier Transform Spectroscopy (Nobel Lecture)[1]

Richard R. Ernst

Laboratorium für Physikalische Chemie, Eidgenössische Technische Hochschule ETH-Zentrum 8092 Zurich, Switzerland

Contents

I. Introduction

The world of the nuclear spins is a true paradise for theoretical and experimental physicists. It supplies, for example, most simple test systems for demonstrating the basic concepts of quantum mechanics and quantum statistics, and numerous textbook-like examples have emerged. On the other hand, the ease in handling nuclear spin systems predestines them for the testing of novel experimental concepts. Indeed, the universal procedures of coherent spectroscopy have been developed predominantly within nuclear magnetic resonance (NMR)

and have found widespread application in a variety of other fields.

Several key experiments of magnetic resonance have already been honored by Nobel prizes in physics, starting with the famous molecular-beam experiments by Isidor I. Rabi (1-3) acknowledged in 1944, followed by the classical NMR experiments by Edward M. Purcell (4) and Felix Bloch (5,6), honored with the 1952 prize, and the optical detection schemes by Alfred Kastler (7), leading to a prize in 1966. Some further Nobel prize winners in Physics have been associated in various ways with magnetic resonance: John H. Van Vleck developed the theory of dia- and paramagnetism and introduced the moment method into NMR; Nicolaas Bloembergen had a major impact on early relaxation theory and measurements; Karl Alex Müller contributed significantly to electron paramagnetic resonance; Norman F. Ramsey is responsible for the basic theory of chemical shifts and J couplings; and Hans G. Dehmelt developed pure nuclear quadrupole resonance.

But not only for physicists is nuclear magnetic resonance of great fascination. More and more chemists, biologists and medical doctors discover NMR spectroscopy, not so much for its conceptual beauty but for its extraordinary usefulness. In this context, a great number of magnetic resonance tools have been invented to enhance the power of NMR in view of a variety of applications (8-15). This Nobel lecture provides a glimpse behind the scenes in an NMR toolmaker's workshop.

Nuclear spin systems possess unique properties that predestine them for studies of molecules:

1) The atomic nuclei serving as sensors are extremely well localized, with a diameter of a few femtometers, and can report on local affairs in their immediate vicinity. It is thus possible to explore molecules and matter in great detail.

2) The interaction energy of the sensors with the environment is extremely small, less than 0.2 J mol^{-1}, corresponding to the thermal energy at 30 mK. The monitoring of molecular properties is thus virtually perturbation-free. Nevertheless, the interaction is highly sensitive to the local environment.

3) Information on the structure of molecules can be obtained from nuclear pair interactions: Magnetic dipole-dipole interactions provide distance information, while scalar J couplings allow one to determine dihedral angles.

At first glance, it may be astonishing that it is possible to accurately determine internuclear distances by radio frequencies with wavelengths $\lambda \approx 1$ m, since this seemingly violates the quantum mechanical uncertainty relation, $\sigma_q \cdot \sigma_p \geq \hbar/2$, with the linear momentum $p = 2\pi\hbar/\lambda$, as it applies to scattering experiments or to a microscope. It is important that in magnetic resonance the geometric information is encoded in the spin Hamiltonian, $\mathcal{H} = \mathcal{H}(\mathbf{q}_1, \ldots, \mathbf{q}_k)$, where $\mathbf{q}_k$ is the nuclear coordinates. An accurate structure determination, therefore, boils down to an accurate energy measurement that can be made as precise as desired, provided that the observation time t is extended according to $\sigma_E \cdot t \geq \hbar/2$. An upper limit of t is in practice given by the finite lifetime of the energy eigenstates due to relaxation processes. Thus, the accuracy of NMR measurements is not restricted by the wavelength but rather by lifetimes limited by relaxation processes.

The information content of a nuclear spin Hamiltonian and the associated relaxation superoperator of a large molecule, for example a protein, is immense: It is possible to determine the frequencies of the chemical shifts of hundreds of spins in a molecule to an accuracy of 16-18 bits. Internuclear distances for thousands of proton pairs can be measured to about 0.1 Å. Several hundred dihedral angles in a molecule can be determined with an uncertainty of less than 10°.

The weakness of the nuclear spin interactions, so far described as an advantage, leads on the other hand to severe problems in detection. Large numbers of spins are required to discriminate the weak signals from noise. Under optimum conditions with modern high-field NMR spectrometers, 10^{14}–10^{15} spins of one kind are needed to detect a signal within a measurement time of one hour. The low signal-to-noise ratio is the most limiting handicap of NMR. Any increase by technical means would significantly extend the possible range of NMR applications.

This clearly defines the two goals that had to be achieved during the past three decades to promote NMR as a practical tool for molecular structure determination: 1) Optimization of the signal-to-noise ratio; 2) Development of procedures to cope with the enormous amount of inherent information on the molecule under investigation.

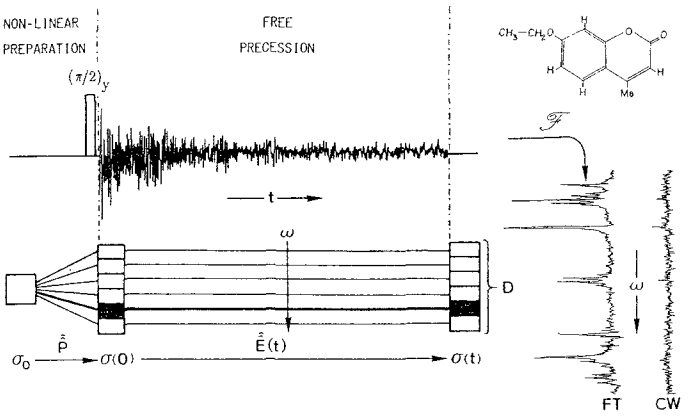

Figure 1: Schematic representation of pulse FT spectroscopy illustrated by the 60 MHz ^{1}H NMR spectrum of 7-ethoxy-4-methylcoumarin (22). An initial $(\pi/2)_y$ rf pulse, represented by the rotation superoperator $\hat{\hat{P}}$, excites the transverse magnetization $\sigma(0)$ from the equilibrium state σ_0. Free precession of all coherences in parallel under the evolution superoperator $\hat{\hat{E}}(t)$ leads to the final state $\sigma(t)$. Detection with the detection operator **D** produces the FID shown (sum of 500 scans) which, after Fourier transformation $\mathcal{F}$ provides the spectrum FT. For comparison, a continuous-wave (CW) spectrum is shown which was also recorded in 500 s under identical conditions.

II. One-Dimensional Fourier Transform Spectroscopy

A major improvement in the signal-to-noise ratio of NMR spectra was achieved in 1964 by the conception of Fourier transform (FT) spectroscopy. The basic principle–parallel data acquisition, leading to the multiplex advantage–was applied already by Michelson in 1891 in optical spectroscopy (16) and explicitly formulated by Fellgett in 1951 (17). However, the approach used in optics, spatial interferometry, is unsuited for NMR spectroscopy, since an interferometer with the necessary resolution would require a pathlength of at least 3×10^8 m.

Weston A. Anderson at Varian Associates in Palo Alto was experimenting in the early sixties with a mechanical multiple-frequency generator, the "wheel of fortune", which was conceived to simultaneously excite the spin system with N frequencies, in order to shorten the performance time of an experiment by a factor N, by recording the response of N spectral elements in parallel (18). It was soon recognized that more elegant solutions were needed for commercial success.

Numerous possibilities are conceivable for the generation of a broad-band frequency source that allows the simultaneous irradiation of all of the spins of a spin system. We mention four schemes: 1) Radio-frequency pulse excitation, 2) stochastic random noise excitation, 3) rapid scan excitation, 4) excitation by a computer-synthesized multiple-frequency waveform. For each method, a different type of data processing is required to derive the desired NMR spectrum.

The application of radio-frequency (rf) pulse excitation was suggested by Weston A. Anderson to the author for a detailed experimental study in 1964 (19-21). The experiment is outlined in Figure 1. To the sample that is polarized in a static magnetic field along the z-axis, an rf pulse is applied along the y-axis that rotates the magnetization vectors $\mathbf{M}_k$ of all spins $\mathbf{I}_k$ by $\pi/2$ into an orientation perpendicular to the static field. In the arrow notation (23) with the acting operator, here a $(\pi/2)_y$ rotation, on the top of the arrow this is expressed by eqn. 1.

$$M_{kz} \xrightarrow{(\pi/2)_y} M_{kx} \qquad (1)$$

The subsequent free induction decay (FID) consists of the superposition of all eigenmodes of the system. The operator D of an observable is used to detect the signal that is Fourier-transformed to separate the different spectral contributions. Figure 1 shows an early example of FT NMR spectroscopy on the sample 7-ethoxy-4-methylcoumarin for which 500 FIDs were coadded and Fourier-transformed to produce the FT spectrum shown (22). A continuous wave (cw) spectrum obtained by the slow passage through the frequency range was recorded in the same total time of 500 s and is also shown in Figure 1 for comparison of the signal-to-noise ratios.

To please the more mathematically inclined reader, the experiment can also be expressed by the evolution of the density operator $\boldsymbol{\sigma}(t)$ under the preparation superoperator $\hat{\hat{P}} = \exp\{-i\hat{\hat{F}}_y\pi/2\}$ and the evolution superoperator $\hat{\hat{E}}(t) = \exp\{-i\hat{\hat{\mathcal{H}}}t - \hat{\hat{\Gamma}}t\}$. The superoperator $\hat{\hat{F}}_y$ is defined by $\hat{\hat{F}}_y\ \mathrm{A} = [\mathrm{F}_y, \mathrm{A}]$

with $F_y = \sum_k I_{ky}$ where I_{ky} is a component angular momentum operator of spin k. $\hat{\hat{\mathcal{H}}}$ is the Hamiltonian commutator superoperator, $\hat{\hat{\mathcal{H}}}A = [\mathcal{H}, A]$ and $\hat{\hat{\Gamma}}$ is the relaxation superoperator. The expectation value $<\mathbf{D}>(t)$ of the observable operator D is then given by eqn. 2, where $\boldsymbol{\sigma}_0$ represents the density operator of the spin system in thermal equilibrium.

$$< \mathbf{D} > (t) = \mathrm{Tr}\{\mathbf{D}\hat{\hat{\mathrm{E}}}(t)\hat{\hat{\mathrm{P}}}\boldsymbol{\sigma}_0\} \qquad (2)$$

The reduction in performance time for *one* spectrum is determined by the number of spectral elements N, that is, the number of significant points in the spectrum, roughly given by $N = F/\Delta f$, where F is the total width of the frequency range and Δf a typical linewidth of a signal. A corresponding increase in the signal-to-noise ratio of $\sqrt{N}$ per unit time can be obtained by coadding an appropriate number of FID signals originating from a repeated pulse experiment. The gain in signal-to-noise can be appreciated from Figure 1.

It has been known for a long time that the frequency response function (spectrum) of a linear system is the Fourier transform of the impulse response (FID). This was already implicitly evident in the work of Jean Baptiste Joseph Fourier who in 1822 investigated the heat conduction in solid bodies (24). In 1957 Lowe and Norberg proved this relation to hold also for spin systems despite their strongly nonlinear response characteristics (25).

Stochastic testing of unknown systems by white random noise was proposed in the forties by Norbert Wiener (26). One could say that the color of the output noise carries the spectral information on the investigated system. The first applications of random noise excitation in NMR spectroscopy were proposed independently by Russel H. Varian (27) and by Hans Primas (28,29) for broad-band excitation and broad-band decoupling, respectively. The first successful experiments using random noise irradiation led to heteronuclear "noise decoupling" (30,31), a method that proved to be essential for the practical success of ^{13}C NMR spectroscopy in chemical applications.

In 1970, Reinhold Kaiser (32) and the author (33) independently demonstrated stochastic resonance as a means to improve the signal-to-noise ratio of NMR experiments by broad-band irradiation. Here, the computed cross-correlation function (eqn. 3) of the input noise $n_i(t)$ and the output noise $n_o(t)$ is equivalent to the FID of pulse FT spectroscopy.

$$c_1(\pi) = \overline{n_o(t)n_i(t-\tau)} \qquad (3)$$

This is illustrated in Figure 2 for fluorine resonance of 2,4-difluorotoluene. A binary pseudo-random sequence with a maximal white spectrum is used for excitation. Its advantages are the predictable spectral properties and the constant rf power. The low peak-power puts less stringent requirements on the electronic equipment. Disadvantages arise from the simultaneous irradiation and detection which can lead to line-broadening effects absent in pulse FT spectroscopy in which perturbation and detection are separated in time. A further disadvantage, when real random noise is used, is the probabilistic nature of the response which requires extensive averaging to obtain a stable mean value. Higher order correlation functions, such as eqn. 4 allow also the characterization of nonlinear transfer properties of the investigated system (26).

$$c_3(\tau_1, \tau_2, \tau_3) = \overline{n_o(t)n_i(t-\tau_1)n_i(t-\tau_2)n_i(t-\tau_3)} \qquad (4)$$

This has been exploited extensively by Blümich and Ziessow for NMR measurements (34,35).

A third approach, rapid scan spectroscopy, initially proposed by Dadok and Sprecher (36), achieves a virtually simultaneous excitation of all spins by a rapid sweep through the frequency range (37,38). The resulting spectrum is strongly distorted, but can be corrected mathematically because of the deterministic nature of the distortions. Correction amounts to convolution with the signal of a single spin measured under identical conditions or simulated on a computer. An example is given in Figure 3. It is interesting to note how similar a rapid scan spectrum is to an FID except for the successively increasing oscillation frequency.

Finally, it is possible by computer synthesis to compute an excitation function with a virtually arbitrary excitation profile. This was originally utilized for decoupling purposes by Tomlinson and Hill (39), but is also the basis for composite pulse excitation schemes that have proved to be very powerful (40,41).

Among the broad-band excitation techniques, pulse excitation is the only one that allows for a rig-

orous analytical treatment irrespective of the complexity of the spin system. It does not lead to any method-inflicted line broadening as in stochastic resonance nor to correction-resistant signal distortions as in rapid scan spectroscopy of coupled spin systems (38). Pulse FT spectroscopy is conceptually and experimentally simple, and last but not least, it can easily be expanded and adapted to virtually all conceivable experimental situations. Measurements of relaxation times, for example, require just a modified relaxation-sensitive preparation sequence, such as a $\pi - \pi/2$ pulse pair for T_1 measurements (42) and a $\pi/2 - \pi$ pulse pair for T_2 measurements (43). Also the extension to the investigation of chemical exchange using the saturation-transfer experiment of Forsén and Hoffman (44) is easily possible.

It should be mentioned at this point that pulse NMR experiments were suggested already by Felix Bloch in 1946 in his famous paper (6), and the first time-domain magnetic resonance experiments were performed in 1949 by H. C. Torrey (45) and, in particular, by Erwin L. Hahn (46-48), who may be regarded as the true father of pulse spectroscopy. He invented the spin-echo experiment (46) and devised extremely important and conceptually beautiful solid-state experiments (49,50).

Pulse FT spectroscopy has not only revolutioned high-resolution liquid-state NMR spectroscopy, but it has unified NMR methodology across all fields, from solid-state resonance, through measurements of relaxation times, to high-resolution NMR, with numerous spillovers also into other fields such as ion cyclotron resonance (51), microwave spectroscopy (52), and electron paramagnetic resonance (53). It also provided the germ for the development of multidimensional NMR spectroscopy.

III. Two-Dimensional Fourier Transform Spectroscopy

As long as purely spectroscopic measurements are made for the determination of the eigenfrequencies or normal modes of a system, one-dimensional (1D) spectroscopy is fully adequate. In NMR spectroscopy, this applies to the measurement of the chemical shifts that characterize the local chemical environment of the different nuclei. However, no information can be obtained in this manner on the spatial relationships between the observed nuclei.

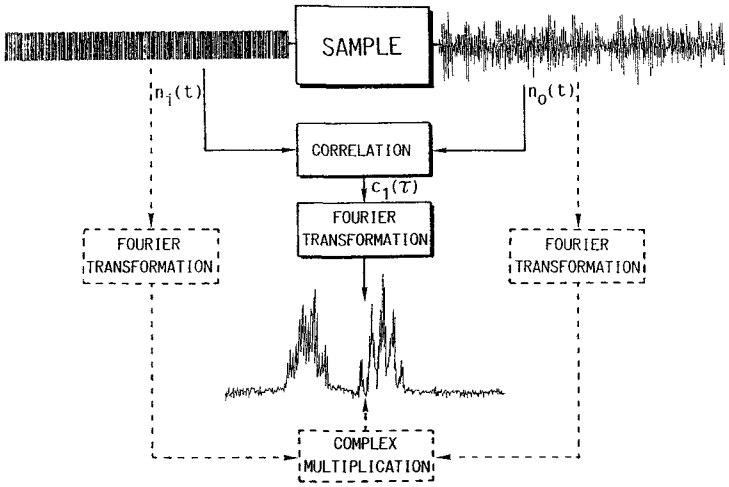

Figure 2: Schematic representation of stochastic resonance illustrated by the 56.4 MHz ^{19}F NMR spectrum of 2,4-difluorotoluene (33). Excitation with a binary pseudo-random sequence $n_i(t)$ 1023 points in length generates the response $n_o(t)$. Cross-correlation of the two signals produces $c_1(\tau)$ which, after Fourier transformation, delivers the spectrum shown. In an alternative procedure, which has actually been used in this case, the individual Fourier transforms of $n_i(t)$ and $n_o(t)$ are computed, and the complex conjugate $\mathcal{F}\{n_i(t)\}^*$ is multiplied by $\mathcal{F}\{n_o(t)\}$ to obtain the same spectrum.

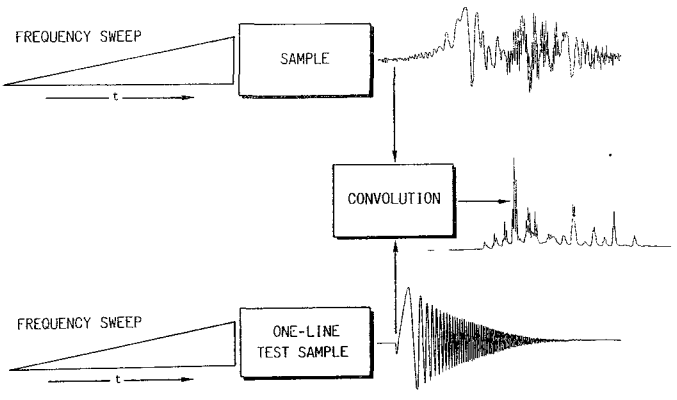

Figure 3: Schematic representation of rapid scan spectroscopy. The highly distorted sample spectrum obtained by a rapid frequency sweep of the frequency during the time t can be corrected by convolution with the equally sweep-distorted spectrum of a one-line test sample.

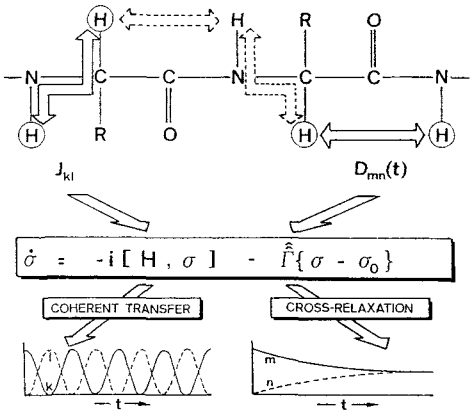

Figure 4: The two pair-interactions relevant in NMR spectroscopy. The through-bond scalar J_{kl} coupling contributes to the Hamiltonian and leads to a coherent transfer (A) of spin order between spins I_k and I_l. The time-modulated through-space dipole-dipole interaction $D_{mn}(t)$ causes multiexponential cross relaxation (B) between spins I_m and I_n. The two interactions allow a sequential assignment of the resonances of neighboring spins in the peptide fragment shown and the determination of structure parameters. The three-bond J coupling is a measure for the dihedral angle about the central bond, the dipole-dipole interaction for internuclear distances.

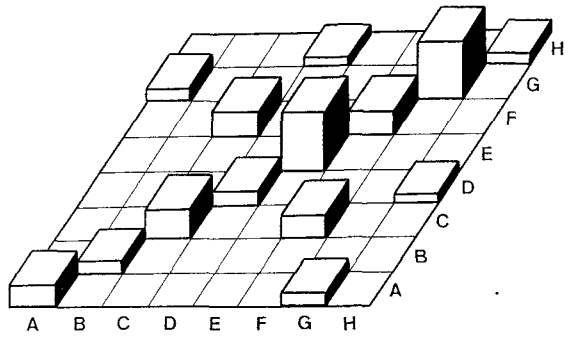

Figure 5: Schematic correlation diagram for the representation of pair interactions of nuclear spins.

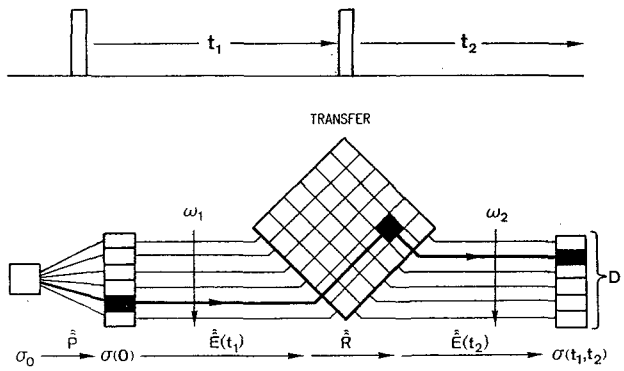

Figure 6: Schematic representation of a 2D experiment, here with a simple two-pulse sequence. The first pulse excites coherences that precess during t_1 and are transferred by the second pulse to different transitions where the coherences continue to precess with a new frequency. The 2D spectrum obtained by a 2D Fourier transformation of $<\mathbf{D}>(t_1, t_2)$ is a visual representation of the transfer matrix R.

There are two important pair interactions in nuclear spin systems, the scalar through-bond electron-mediated spin-spin interaction (J coupling) and the through-space magnetic dipole-dipole interaction (Figure 4). The J coupling is described by the scalar term $\mathcal{H}_{kl} = 2\pi J_{kl}\mathbf{I}_k\mathbf{I}_l$ in the spin Hamiltonian. It is responsible for the multiplet splittings in high-resolution spectra of liquids. Under suitable conditions, it can lead to an oscillatory transfer of spin order between the two spins $\mathbf{I}_k$ and $\mathbf{I}_l$. The magnetic dipole-dipole interaction D_{mn}, on the other hand, is represented by a traceless tensor of second rank. Its average in isotropic solution is zero, and it can lead to signal splitting only in anisotropic media. However, its time modulation causes relaxation processes also in isotropic solution that are responsible for a multiexponential recovery of the spins to thermal equilibrium after a perturbation. Knowledge of these interactions allows one to deduce geometric relations in the molecule in solution (54,55) and arrangements of atoms in solids. In the optimum case, a complete three-dimensional structure of a molecule can be deduced (56).

Although these interactions affect 1D spectra, special techniques are needed for their measurement. In the approximation of a linear response, it is impossible by first principles to distinguish two independent signals from a doublet caused by a spin-spin interaction. Experiments to explore the nonlinear response properties of nuclear spin systems have been known since the fifties. In saturation studies with strong rf fields several spins belonging to the same coupled spin system are excited simultaneously yielding multiple-quantum transitions that

contain connectivity information (57). Particularly fruitful were double- and triple-resonance experiments in which two or three rf fields are applied simultaneously, resulting in decoupling and spin-tickling effects (58-60).

The early multiple-resonance experiments have in the meantime been replaced by multidimensional experiments. Pair interactions among spins are most conveniently represented in terms of a correlation diagram as shown in Figure 5. This suggests the recording of a "two-dimensional spectrum" that establishes such a correlation map of the corresponding spectral features. The most straightforward approach may be a systematic double-resonance experiment whose result can be represented as an amplitude $S(\omega_1, \omega_2)$ which depends on the frequencies ω_1 and ω_2 of the two applied rf fields (8,58).

A new approach to measuring two-dimensional (2D) spectra was proposed by Jean Jeener in 1971 (61). He suggested a 2D FT experiment consisting of two $\pi/2$ pulses with a variable time t_1 between the pulses and the time variable t_2 measuring the time elapsed after the second pulse as shown in Figure 6; this is an expansion of the principles illustrated in Figure 1 (see also Fig. 10a). Measuring the response $s(t_1, t_2)$ of the two-pulse sequence which is Fourier-transformed with respect to both time variables produces a two-dimensional spectrum $S(\omega_1, \omega_2)$ of the desired form (62,63).

This two-pulse experiment by Jean Jeener is the progenitor of a whole class of 2D experiments (8,63) which can also easily be expanded to multidimensional spectroscopy. Each 2D experiment, as shown in Figures 6 and 7, starts with a preparation pulse sequence $\hat{\hat{\mathrm{P}}}$, which excites coherences, that is, coherent superpositions represented by the density operator $\boldsymbol{\sigma}(0)$, that are allowed to precess for an evolution time t_1 under the evolution superoperator $\hat{\hat{\mathrm{E}}}(t_1)$. During this period, the coherences are frequency-labeled, so to speak. The subsequent mixing sequence $\hat{\hat{\mathrm{R}}}$ performs a controlled transfer of coherence to different nuclear spin transitions that evolve during the detection period as a function of t_2 under the evolution superoperator $\hat{\hat{\mathrm{E}}}(t_2)$. Detection is performed with the detection operator $\mathbf{D}$ in analogy to Figure 1, leading to eqn. 5.

$$< \mathbf{D} > (t_1, t_2) = \mathrm{Tr}\{\mathbf{D}\hat{\hat{\mathrm{E}}}(t_2)\hat{\hat{\mathrm{R}}}\hat{\hat{\mathrm{E}}}(t_1)\hat{\hat{\mathrm{P}}}\sigma_0\} \quad (5)$$

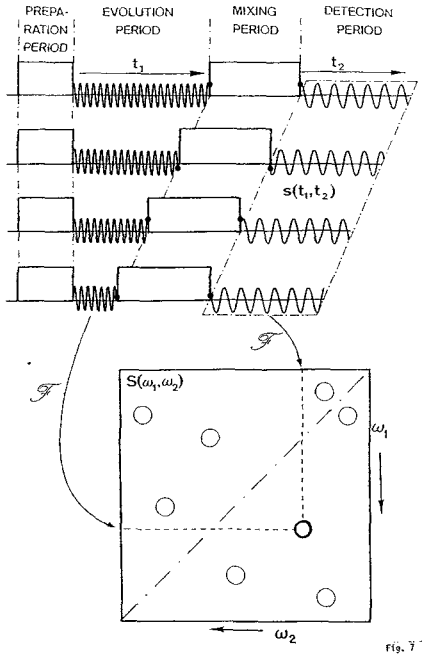

Figure 7: Schematic representation of a general 2D experiment consisting of preparation, evolution, mixing, and detection periods. The duration t_1 of the evolution period is varied systematically from experiment to experiment. The resulting signal $s(t_1, t_2) \propto < \mathbf{D} > (t_1, t_2)$ is Fourier-transformed in two dimensions to produce the 2D spectrum $S(\omega_1, \omega_2)$.

It is not sufficient to perform a single two-pulse experiment. To obtain the necessary data $<\mathbf{D}>$ (t_1, t_2) to compute a 2D spectrum $S(\omega_1, \omega_2)$, it is required to systematically vary t_1 in a series of experiments and to assemble a 2D data matrix that is then Fourier-transformed in two dimensions as is indicated schematically in Figure 7. The resulting 2D spectrum correlates the precession frequencies during the evolution period with the precession frequencies during the detection period, and is a vivid and easily interpretable representation of the mixing process. Diagonal and cross peaks are measures for the elements of the transfer matrix of the mixing pulse sequence in Figure 6.

Among the numerous transfer processes that can be represented in this manner, the most important ones (8) are 1) the scalar J coupling leading to 2D correlation spectroscopy abbreviated as COSY, 2) internuclear cross relaxation leading to 2D nuclear Overhauser effect spectroscopy abbreviated as NOESY, and 3) chemical exchange leading to 2D exchange spectroscopy abbreviated as EXSY.

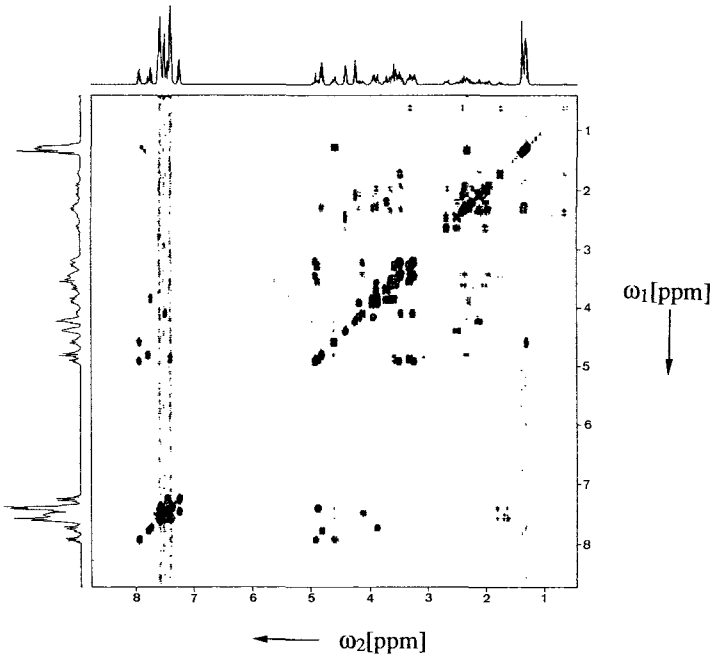

Figure 8: Phase-sensitive 400 MHz ^{1}H COSY spectrum of antamanide (**1**) in chloroform (at 250 K) in a contour-line representation. Positive and negative contours are not distinguished. The spectrum was recorded by Dr. Martin Blackledge.

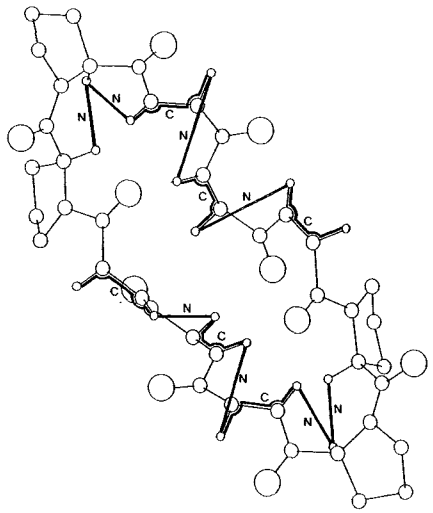

Figure 9: Assignment of the protons of the backbone of antamanide (**1**) by the combination of COSY (C) and NOESY (N) cross peaks. The missing NH protons in the four proline residues break the chain of sequential C–N connectivities.

The COSY transfer, which proceeds through J coupling, is truly a quantum mechanical effect that does not find a satisfactory classical explanation. By means of a single $(\pi/2)_x$ rf mixing pulse, as in Figure 6, it is possible to transfer coherence of spin k, which is antiphase with respect to spin l and represented in the density operator by the operator term $2\mathbf{I}_{ky}\mathbf{I}_{lz}$ into coherence of spin l, which is antiphase with respect to spin k, represented by $-2\mathbf{I}_{kz}\mathbf{I}_{ly}$ (eqn. 6), whereby each factor of the product spin-operator can be considered to be rotated by $\pi/2$ about the x-axis.

$$2\mathbf{I}_{ky}\mathbf{I}_{lz} \xrightarrow{(\pi/2)_x} -2\mathbf{I}_{kz}\mathbf{I}_{ly} \tag{6}$$

Antiphase coherence of the type $2\mathbf{I}_{ky}\mathbf{I}_{lz}$ is only formed during the evolution period when there is a direct spin-spin coupling between the spins $\mathbf{I}_k$ and $\mathbf{I}_l$ (eqn. 7).

$$\mathbf{I}_{kx} \xrightarrow{2\pi J_{kl}\mathbf{I}_{kz}\mathbf{I}_{lz}t_1} \mathbf{I}_{kx}\cos(\pi J_{kl}t_1) + 2\mathbf{I}_{ky}\mathbf{I}_{lz}\sin(\pi J_{kl}t_1) \tag{7}$$

This implies that in a two-dimensional correlation spectrum there are cross peaks only between directly coupled spins (as long as the approximation of weak coupling holds). It is obvious from eqn. 7 that there is no net coherence transfer, e.g. $\mathbf{I}_{kx} \rightarrow \mathbf{I}_{lx}$, and the cross-peak integral must disappear. In other words, there is an equal number of cross-peak multiplet lines with positive and negative intensity.

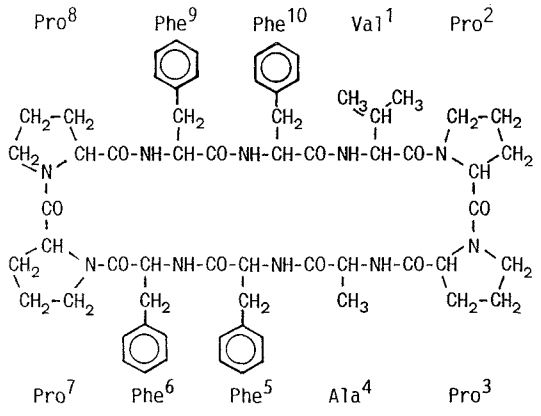

A COSY spectrum, such as the one shown in Figure 8 for the cyclic decapeptide antamanide (**1**) can be used to find pairs of spins belonging to the same coupling network of an amino acid residue in

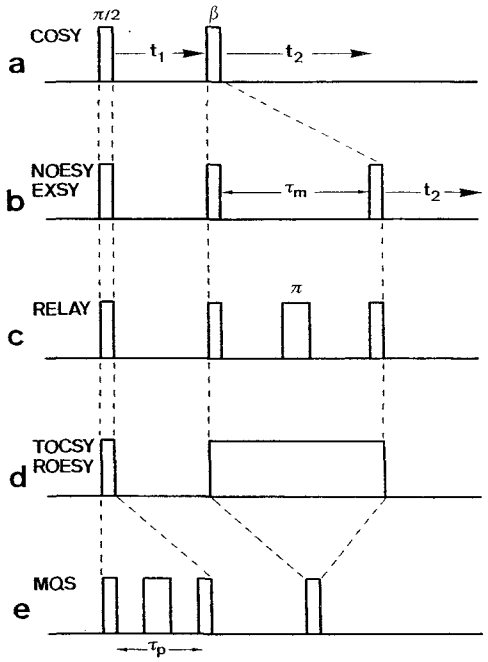

Figure 10: Pulse sequences for some of the most useful homonuclear 2D experiments: a) COSY, b) NOESY or EXSY, c) relayed COSY, d) TOCSY or ROESY in the rotating coordinate system, e) multiple-quantum spectroscopy.

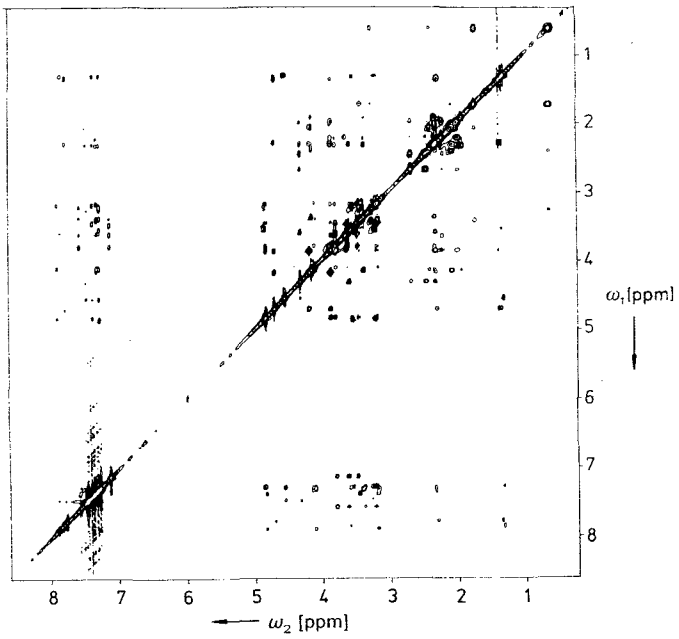

Figure 11: 400 MHz ^{1}H NOESY spectrum of antamanide (**1**) in chloroform (at 250 K) in a contour-line representation. The spectrum was recorded by Dr. Martin Blackledge.

the molecule. All intense cross peaks arise from couplings over two and three bonds that allow, first of all, the assignment of the pairs of NH and $C_\alpha H$ along the polypeptide backbone (backbone protons), as indicated by C in Figure 9 for the six amino acid residues with NH protons. In addition, it is also possible to assign the protons in the side chains.

The transfers of NOESY and EXSY experiments involve incoherent, dissipative processes that bring the system back to equilibrium in an exponential or multiexponential manner after an initial perturbation. They require an extended mixing time during which the random processes are given a chance to occur. Both processes can be investigated with the same three-pulse scheme (Figure 10b) (8,64-67). The mixing period is bracketed by two $\pi/2$ pulses that transform coherence into static spin-order and back into coherence. The exchange processes transfer the spin order between different spins or between different chemical species, respectively. This type of transfer can be understood on the basis of classical kinetic models. The resulting 2D spectrum represents a kinetic matrix with cross-peak intensities proportional to the exchange rate constants of pseudo-first-order reactions.

For the NOESY transfer, the exchange rate constants are given by the cross-relaxation rate constants, which are due to magnetic dipole-dipole interactions, and are proportional to $1/r_{kl}^6$ for nuclear pairs I_k and I_l, and depend on the correlation time τ_c of the tumbling of the molecules in solution. The distance dependence can be used to measure relative or, if τ_c is known, absolute distances in molecules. The NOESY cross peaks thus allow the identification of neighboring protons in a molecule – important, for example, in identifying protons that belong to adjacent amino acid residues in peptides.

A NOESY spectrum of antamanide (**1**) is given in Figure 11. The sequential backbone protons of adjacent amino acid residues with NOESY cross peaks are marked in Figure 9 with N. It is seen in Figure 9 that these together with the protons with *J*- cross peaks from the COSY spectrum (Figure 8) form two unbroken chains of connectivities that can be used for the identification of the backbone protons. The two chains are not joined because of the absence of NH protons in the four proline residues. The general assessment procedure of proton resonance frequencies based on COSY and NOESY spectra has been established by Wüthrich

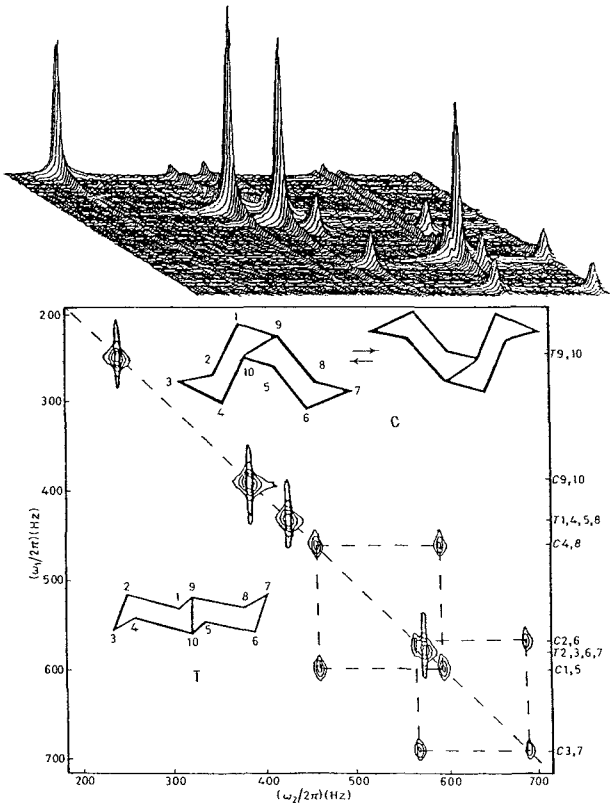

Figure 12: 2D ^{13}C EXSY spectrum of a mixture of *cis*- and *trans*-decalin recorded at 22.5 MHz and 241 K (76). Top: Three-dimensional representation (stacked plot). Bottom: A contour-line representation with the assignment of the peaks.

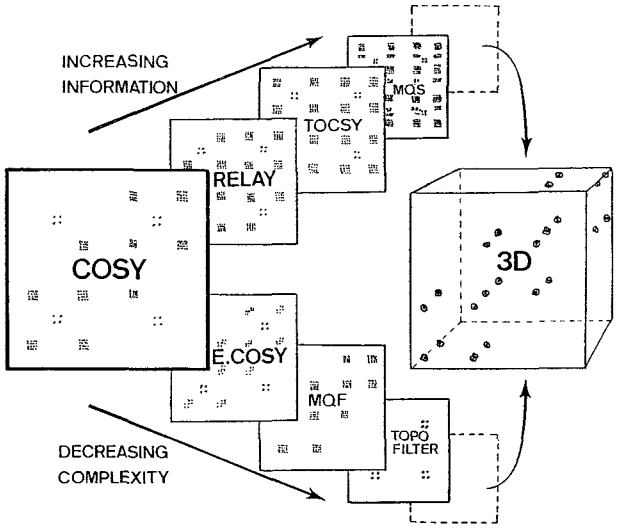

Figure 13: Extensions of the standard COSY experiment. Relayed correlation, total correlation spectroscopy (TOCSY), and multiple-quantum spectroscopy (MQS) increase the information content, while exclusive correlation (E. COSY), multiple-quantum filtering (MQF), and spin-topology filtration reduce the complexity. Both avenues can lead to three-dimensional spectroscopy.

and his research group (56).

Based on a complete or partial set of assigned resonances, it is then possible to deduce information on the molecular structure. Each NOESY cross-peak intensity provides an internuclear distance that can be used in a manual or computerized process to construct a molecular model compatible with the experimental data. In this process it is also possible to employ scalar coupling constants extracted from COSY-type spectra (most conveniently from E. COSY spectra, as mentioned later). According to the Karplus relations (54), there is a relation between vicinal coupling constants and dihedral angles. Ingenious computer procedures to determine molecular structures based on NMR data were first developed by Kurt Wüthrich and his research team and tested on a large number of small to medium-size proteins (56, 68-71). At present, mainly two computer algorithms for the structure determination are in use – the distance-geometry algorithm (72,73) and modifications of it, and the restrained molecular-dynamics algorithm (74,75), again with many variations. The structural problem in antamanide (**1**) will be discussed later, as it involves intramolecular dynamic processes that complicate the situation.

Cross peaks in a NOESY-type exchange spectrum can also originate from chemical exchange; the three-pulse experiment of Figure 10b is indeed well suited for the investigation of chemical exchange networks (64,65,76). A distinction of the two types of signals is not possible by inspection of a single 2D spectrum. However, variable-temperature studies are often conclusive. At sufficiently low temperatures at which chemical exchange becomes slow, only NOESY cross peaks should remain. The two types of signals may also be distinguished in experiments with rotating coordinate systems as mentioned in the next section.

The ^{13}C NMR spectrum of a mixture of *cis*- and *trans*-decalin in Figure 12 is typical for a spectrum

showing chemical exchange. The spectrum gives evidence of the well-known conformational stability of *trans*-decalin, whereas for *cis*-decalin four pairs of carbon spins are involved in a conformational exchange process, giving raise to two pairs of cross peaks (76).

IV. Modified Two-Dimensional FT-NMR Experiments

Starting from the two prototypical 2D FT NMR experiments, numerous modified, expanded, and improved experiments have been suggested. Many of them have found a place in the arsenal of routine methods for the NMR spectroscopist. A first category of experiments, represented in the upper part of Figure 13, causes extended correlation through two or more transfer steps: Relayed correlation experiments involve two-step correlation, and total correlation spectroscopy (TOCSY) multiple-step correlation. The latter experiment leads to the important class of rotating frame experiments, including rotating frame Overhauser effect spectroscopy (ROESY) an alternative to NOESY. Finally also multiple-quantum spectroscopy allows one to investigate connectivity in spin systems. A second class of experiments attempts the simplification of spectra by exclusive correlation (E. COSY), multiple-quantum filtering, and spin-topology filtration.

V. Relayed Correlation

In a standard COSY experiment, coherence is transfered exclusively between two directly coupled spins by means of a single mixing pulse. By a sequence of two $\pi/2$ pulses, as in Figure 10c, it is possible to effect a transfer of coherence across two sequential couplings from spin I_k to spin I_l through the relay spin I_r (77,78). For the relation in eqn. 8, $J_{kr}t_1 = J_{kr}\tau_m = J_{rl}\tau_m = 1/2$ is assumed.

$$\mathbf{I}_{kz} \xrightarrow{(\pi/2)\mathbf{I}_{ky}} \mathbf{I}_{kx} \xrightarrow{2\pi J_{kr}\mathbf{I}_{kz}\mathbf{I}_{rz}t_1} 2\mathbf{I}_{ky}\mathbf{I}_{rz} \xrightarrow{(\pi/2)(\mathbf{I}_{kx}+\mathbf{I}_{rx})}$$

$$-2\mathbf{I}_{kz}\mathbf{I}_{ry} \xrightarrow{2\pi J_{kr}\mathbf{I}_{kz}\mathbf{I}_{rz}\tau_m+2\pi J_{rl}\mathbf{I}_{rz}\mathbf{I}_{lz}\tau_m} 2\mathbf{I}_{ry}\mathbf{I}_{lz}$$

$$\xrightarrow{(\pi/2)(\mathbf{I}_{rx}+\mathbf{I}_{lx})} -2\mathbf{I}_{rz}\mathbf{I}_{ly} \qquad (8)$$

During the extended mixing period τ_m, it is thus necessary to refocus the antiphase character of the I_r spin coherences with respect to spin I_k and create antiphase character with respect to spin I_l to allow for a second transfer by the second mixing pulse. Relayed correlation is useful whenever the resonance of the relay spin I_r cannot be identified unambiguously. With a relay experiment it is then nevertheless possible to assign spins I_k and I_l to the same coupling network (e.g. belonging to the same amino acid residue in a polypeptide chain). It is usually advantageous to refocus the effects of the chemical shift precession during the mixing period by incorporating a central π pulse as shown in Figure 10c.

Relayed coherence transfer is illustrated by 300 MHz ^{1}H NMR spectra of the linear nonapeptide buserilin, pyro-Glu-His-Trp-Ser-Tyr-D-Ser-Leu-Arg-Pro-NHCH$_2$CH$_3$. Figure 14a shows a (double-quantum filtered) COSY spectrum and Figure 14b the corresponding relayed COSY spectrum (79). In both spectra, the resonance connectivities for the leucine residue are marked. It is evident that in the COSY spectrum only nearest neighbor protons are connected by cross peaks: NH–C$_\alpha$H, C$_\alpha$H–C$_\beta$H^{1,2}, C$_\beta$H^{1,2}–C$_\gamma$H, and C$_\gamma$H–(C$_\delta$H$_3$)^{1,2}. On the other hand, in the relayed COSY spectrum, also the next-nearest neighbors NH–C$_\beta$H^{1,2} and C$_\beta$H^{1,2}–(C$_\delta$H$_3$)^{1,2} are connected. The third pair of relayed cross peaks C$_\alpha$H–C$_\gamma$H, is weak because of the high multiplicity of the C$_\gamma$H resonance and is not visible in the contour representation of Figure 14b. Similar relayed cross peaks can be found for the other amino acid residues.

VI. Rotating Frame Experiments

By means of an extended mixing pulse sequence, transfer of coherence over an arbitrary number of steps is possible in principle. In particular, continuous wave irradiation leads to the mixing of all eigenmodes of a spin system and correspondingly to transfers of coherence between all of them. This is exploited in total correlation spectroscopy (TOCSY) with the sequence shown in Figure 10d. All spins belonging to the same J-coupling network can be identified with TOCSY (80,81). The accurate matching of the precession frequencies of the

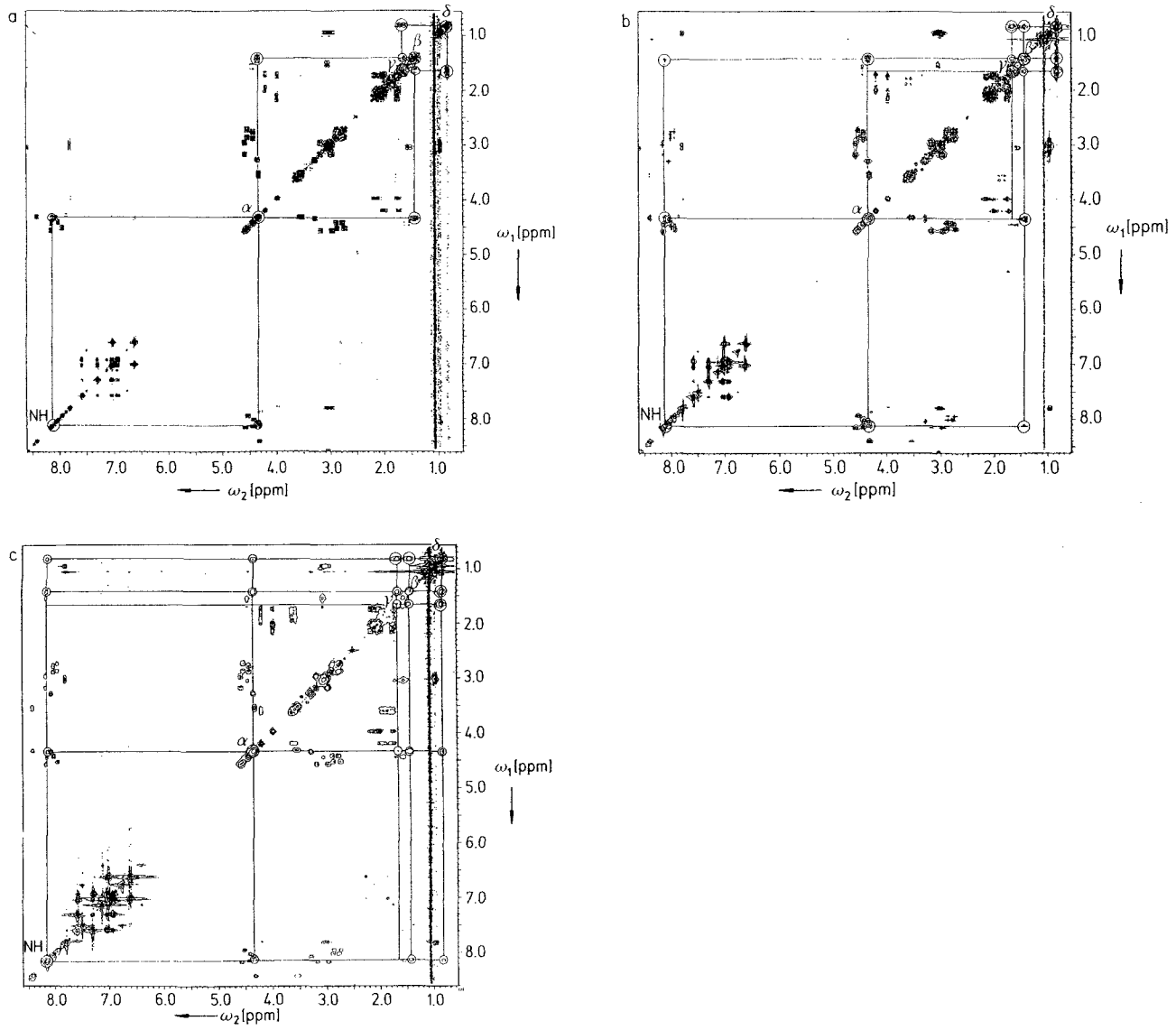

Figure 14: 300 MHz correlation spectra of the nonapeptide buserilin in dimethyl sulfoxide (DMSO). Phase-sensitive spectra with equal representation of positive and negative contours are shown. The resonance connectivities and the positions of the NH, $C_\alpha H$, $C_\beta H$, $C_\gamma H$, and $C_\delta H$ diagonal peaks are indicated for the leucine residue (79). a) Double-quantum filtered COSY spectrum with the sequence from Figure 18. b) Relayed COSY spectrum with the sequence from Figure 10c and $\tau_m = 25$ ms. c) TOCSY spectrum with the sequence from Figure 10d, $\tau_m = 112$ ms, and an MLEV-17 pulse sequence applied during τ_m.

various spins in the presence of a radio frequency field is crucial in enabling an efficient transfer of coherence. Either very strong radio-frequency fields or specially designed pulse sequences are needed for this purpose (81). Coherence transfer is possible when the effective average magnetic field strengths B_k^{eff} in the rotating frame are equal to within a J-coupling constant, $| \gamma(B_k^{eff} - B_l^{eff}) | < | 2\pi J_{kl} |$, corresponding to a strong coupling case in the rotating frame.

The TOCSY experiment is of interest for assignment of proton resonances to individual amino acid residues in a protein. Of particular value is that its transfer rate is enhanced by a factor of 2 in com-

parison to COSY or relayed transfer experiments in the laboratory frame (80). Another property is that, because of the presence of a radio-frequency field, in-phase coherence transfer is possible (eqn. 9), leading to in-phase cross-peak multiplet structures.

$$\mathbf{I}_{kx} \xrightarrow{2\pi J_{kl}\mathbf{I}_k\mathbf{I}_l\tau_m} \mathbf{I}_{lx} \qquad (9)$$

A TOCSY spectrum of buserilin is included in Figure 14c for comparison with the relayed and standard COSY spectra depicted. Again three-step transfers $C_\alpha H$–$(C_\delta H_3)^{1,2}$ and even four-step transfers NH–$(C_\delta H_3)^{1,2}$ are visible here. Some expected cross peaks involving $C_\gamma H$ are missing as before because of the extensive multiplet structure of $C_\gamma H$.

The elimination of the chemical shift precession by the rf irradiation leads not only to the coherent transfer through the J-coupling network, but also to an incoherent transfer of spin order through transverse cross-relaxation. The transverse cross-relaxation terms are, in principle, always present. However, strong differential chemical shift precession of spin pairs normally causes a quenching of the transfer in the sense of first-order perturbation theory. In the presence of a strong rf field, this quenching is no longer operative and transverse cross-relaxation occurs. This is the transfer mechanism of the rotating frame Overhauser effect spectroscopy (ROESY) experiment (82).

ROESY has similar properties as NOESY but differs in the dependence of the cross-relaxation rate constant Γ_{kl} on the correlation time τ_c of the molecular rotational motion that modulates the internuclear dipole-dipole interaction responsible for cross-relaxation (cf. eqns. 10 and 11 where the spectral density J is defined by eqn. 12).

$$\Gamma_{kl}^{\mathrm{NOE}} = \frac{\gamma^4\hbar^2}{10r_{kl}^6}\left(\frac{\mu_0}{4\pi}\right)^2\left[-\frac{1}{2}J(0) + 3J(2\omega_0)\right] \qquad (10)$$

$$\Gamma_{kl}^{\mathrm{ROE}} = \frac{\gamma^4\hbar^2}{10r_{kl}^6}\left(\frac{\mu_0}{4\pi}\right)^2\left[J(0) + \frac{3}{2}J(2\omega_0)\right] \qquad (11)$$

$$J(\omega) = \frac{2\tau_c}{1+(\omega\tau_c)^2} \qquad (12)$$

As usual, ω_0 is the Larmor frequency of the two nuclei with the internuclear distance r_{kl}. Eqns. 10 and 12 imply that $\Gamma_{kl}^{\mathrm{NOE}}$ changes sign for an intermediate correlation time τ_c of $(5/4)^{1/2}\,\omega_0^{-1}$; that is, the cross-relaxation rate becomes small in the neighborhood of this condition. Depending on the viscosity of the solvent and the resonance frequency ω_0, this occurs for globular molecules within a range of molecular mass of 500–2000 Da. $\Gamma_{kl}^{\mathrm{ROE}}$, on the other hand, is less sensitive to τ_c and remains positive for any molecular mass. The ROESY experiment is therefore of advantage for molecules of intermediate size.

In addition, the different sensitivity of NOE and ROE to τ_c allows one to deduce information on intramolecular mobility by comparison of the two measurements (83). An advantage of ROESY over NOESY experiments is that the cross-peak amplitude is negative, while the simultaneously occurring cross peaks due to chemical exchange are positive and allow for an easy distinction as long as the signals do not overlap.

It should be recognized that in the rotating frame coherence transfer through J couplings and cross relaxation occur simultaneously, whereby TOCSY cross peaks are positive and ROESY cross peaks appear with negative amplitude. This complicates the 2D spectra and calls for separation procedures. The suppression of the coherent transfer through J couplings (TOCSY) is easy, because it is only necessary to mismatch the condition $|\,\gamma(B_k^{\mathrm{eff}} - B_l^{\mathrm{eff}})\,| < |\,2\pi J_{kl}\,|$, for example by a slight frequency offset in the presence of not-too-strong rf fields. The cross-relaxation rates are much less sensitive to such a mismatch and a clean ROESY spectrum results.

Obtaining a clean TOCSY spectrum is more demanding because relaxation cannot easily be manipulated. A technique was proposed by C. Griesinger (84), which relies on a combination of eqns. 10 and 11 to set the average cross-relaxation rate constant to zero (eqn. 13). A suitable weighting factor p can be found whenever $\Gamma_{kl}^{NOE} < 0$, that is, for sufficiently large molecules with $\tau_c > (5/4)^{1/2}\omega_0^{-1}$. This requires the magnetization to move on a trajectory that spends a fraction p of time along the z-axis and a fraction (1-p) in the transverse plane. For $\tau_c \to \infty$, one finds $p = 2/3$ for $\overline{\Gamma}_{kl} = 0$. A suitable pulse sequence, a modification of an MLEV-17 spin-locking sequence, has been proposed in ref. (84).

$$\overline{\Gamma}_{kl} = p\Gamma_{kl}^{NOE} + (1-p)\Gamma_{kl}^{ROE} \stackrel{!}{=} 0 \qquad (13)$$

Another optimized sequence, called "Clean CITY", was developed by J. Briand (85). A clean

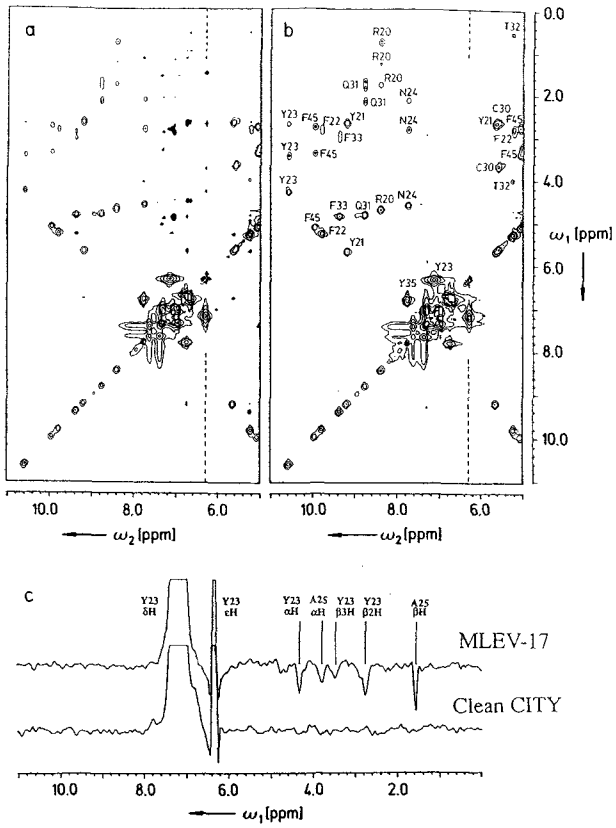

Figure 15: Phase-sensitive 300 MHz ^{1}H TOCSY spectra of 15 mM sample of bovine pancreatic trypsin inhibitor in D_2O recorded with a mixing time of 69 ms (85). a) Mixing process with MLEV-17 pulse sequence. Negative peaks are shown by contours filled in black. b) Mixing process with the Clean CITY pulse sequence. c) Cross sections along ω_1 through the diagonal peak of Tyr$^{23}\varepsilon$H at ω_2 = 6.33 ppm in the spectra a) and b) (marked with broken lines).

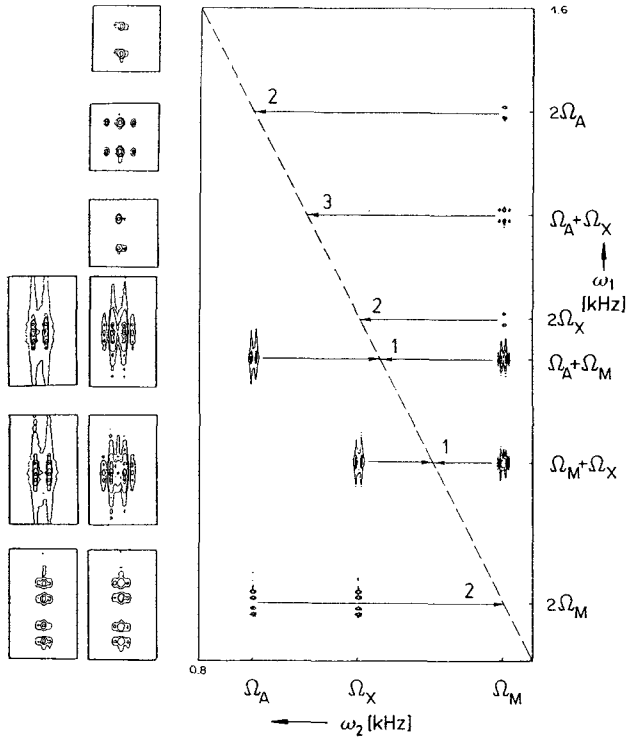

Figure 16: 90 MHz 2D ^{1}H correlation spectrum of [D_3]3-amino-propanol with double-quantum transitions along ω_1 and single-quantum transitions along ω_2. The three types of double-quantum transitions mentioned in the text are indicated. Enlargements of all cross peaks are shown on the left. The spectrum is shown in an absolute value representation (from ref. 89).

TOCSY spectrum of bovine pancreatic trypsin inhibitor (BPTI) using the Clean CITY sequence is compared in Figure 15 with a conventional TOCSY spectrum to demonstrate the efficient suppression of the (negative) ROESY peaks.

VII. Multiple-Quantum Spectroscopy

In the spectroscopy, in general, only those transitions are directly observable for which the observable operator has matrix elements not equal to zero, leading to the so-called allowed transitions. For magnetic resonance in strong magnetic fields with weak cw perturbation or with a free induction decay in the absence of rf, the observable operator of the transverse magnetization $\mathbf{F}_x = \sum_k \mathbf{I}_{kx}$ has matrix elements only between eigenstates of the Hamiltonian differing in the magnetic quantum number M by ± 1. Thus single-quantum transitions are the allowed transitions, while multiple-quantum transitions with $\mid \Delta M \mid > 1$ are forbidden. Multiple-quantum transitions can, however, be induced by strong cw rf fields that cause a mixing of states (8,57) or by a sequence of at least two rf pulses (Fig. 10e)(8,63,86,87). Observation is possible again in the presence of a strong rf field (8,57) or after a further detection pulse (8,63,86,87).

For spin systems with I=1/2, multiple-quantum transitions invariably involve several spins, and multiple-quantum spectra contain information on the connectivity of spins within the *J*-coupling network in analogy to 2D correlation spectra. In particular, the highest order transition allows one to determine the number of coupled spins. Relaxation rate constants of multiple-quantum coherences are dependent on the correlation of the random perturbations affecting the spins involved and provide information on motional processes (88).

A simple instructive example of a 2D double-quantum spectrum is given in Figure 16 to demonstrate the use of multiple-quantum transitions for the assignment of resonances (89). Along ω_1, double-quantum transitions and along ω_2 single-quantum transitions are displayed for the six-spin system of [D_3]3-aminopropanol $DOCH_2CH_2CH_2ND_2$. In general, there are three categories of double-quantum transitions:

1) Double-quantum transitions involving two directly coupled spins. They lead to pairs of cross peaks displaced symmetrically from the double-quantum diagonal ($\omega_1 = 2\omega_2$) with ω_2 coordinates corresponding to the Larmor frequencies of the two spins (e.g. $\omega_1 = \Omega_A + \Omega_M, \Omega_M + \Omega_x$).

2) Double-quantum transitions involving two magnetically equivalent spins. They lead to one or more cross peaks at an ω_1 frequency that intersects the double-quantum diagonal at the ω_2 frequency corresponding to the common Larmor frequency of the two spins (e.g. $\omega_1 = 2\Omega_A, 2\Omega_M, 2\Omega_x$, although the spins are magnetically equivalent only within experimental accuracy).

3) Double-quantum transitions involving two remotely coupled spins. They lead to single cross peaks at an ω_1 frequency that intersects the double quantum diagonal at ω_2 equal to the mean of the two Larmor frequencies (e.g. $\omega_1 = \Omega_A + \Omega_x$). These cross peaks carry information identical to that in relayed correlation spectra.

For the practical application it is essential that a multiple-quantum spectrum never contains an array of strong diagonal peaks. It should be mentioned that a beautiful and useful form of a double-quantum experiment is the 2D INADEQUATE spectroscopy proposed by Bax, Freeman, and Kempsell (90,91). There, only type 1 peaks can arise.

The methods mentioned so far produce additional cross peaks that provide information not accessible with the standard COSY and NOESY experiments. In the following, techniques are discussed that lead to simplified spectra which may facilitate their interpretation.

VIII. Multiple-Quantum Filtering

Selective filtering can be achieved by exciting multiple-quantum coherence, selecting a particular quantum order, and reconverting the selected order into observable magnetization. Depending on the selected order, this leads to multiple-quantum filtering of various orders. The spin-system-selective effect relies on coherence transfer selection rules that limit the allowed transfers for weakly coupled spins (8,92):

1) It is impossible to excite p quantum coherence in spin systems with less than p-coupled spins I=1/2.

2) For the appearance of a diagonal peak of spin I_k in a p-quantum-filtered COSY spectrum, the spin I_k must be directly coupled to at least $p-1$ further spins.

3) For the appearance of the cross peaks between spins I_k and I_l in a p-quantum-filtered COSY spectrum, both spins must simultaneously be coupled to at least $p-2$ further spins.

Violations of these coherence transfer selection rules occur for strong coupling and for certain special relaxation situations (93).

In Figure 17, the effect of four-quantum filtering on various four-spin systems is demonstrated. The sample consists of a mixture of the five compounds *trans*-phenylcyclopropanecarboxylic acid (K_4), DL-isocitric acid-lactone ($P_{3,1}$), 1,1-dichloroethane (S_4), 2-chloropropionic acid (C_4), and D-saccharic acid-1,4-lactone (L_4) with the coupling topologies indicated in Scheme 1 (94).

Figure 17a shows a conventional (double-quantum-filtered) COSY spectrum of the mixture, while in Figure 17b the corresponding four-quantum-filtered spectrum is reproduced. The filtering effect can easily be understood based on the given rules and the coupling topologies shown in

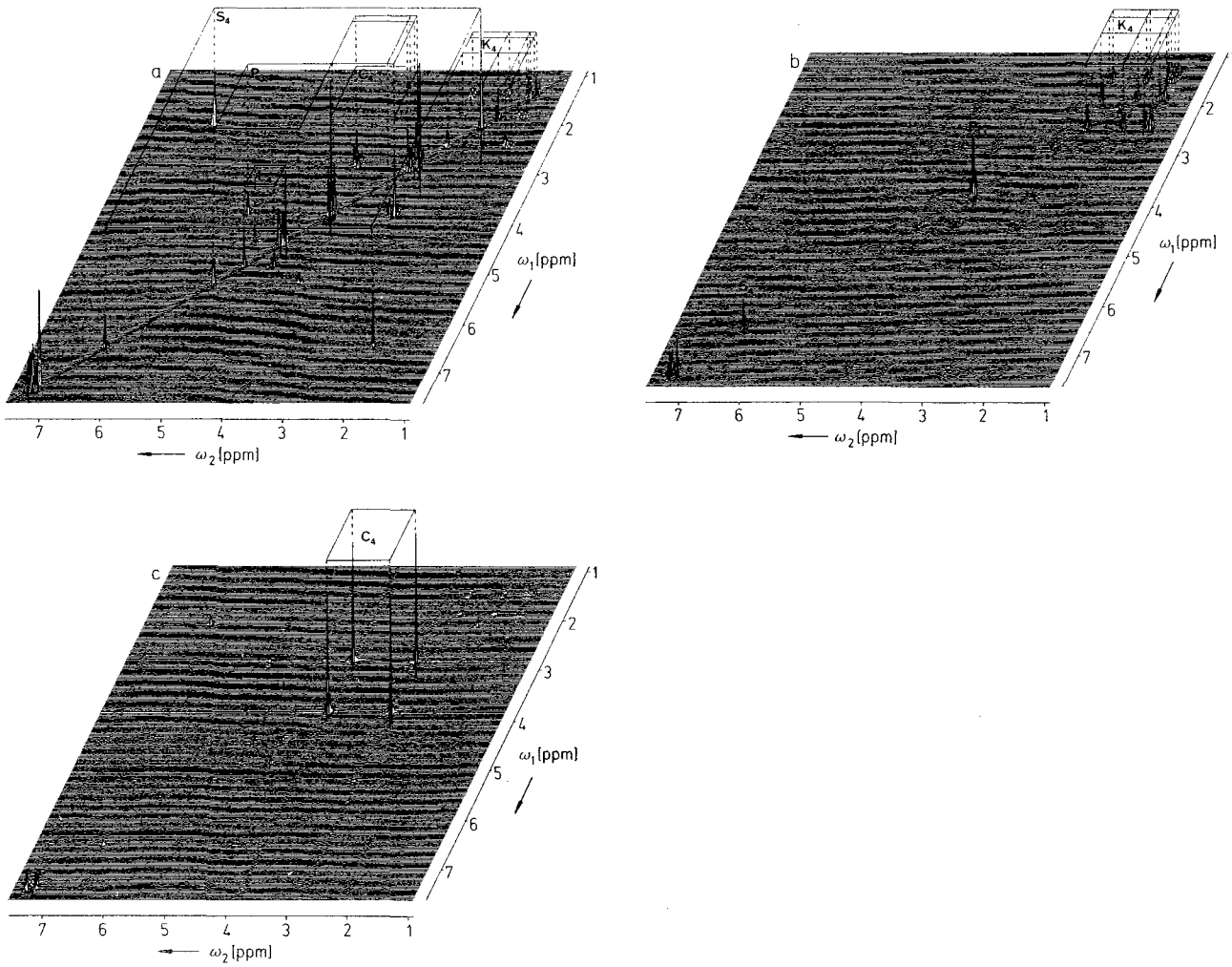

Figure 17: Multiple-quantum-filtered and spin-topology-filtered 300 MHz ^{1}H COSY spectra of a mixture of the compounds from Scheme 1 containing four-spin systems. a) Double-quantum-filtered spectrum obtained with the pulse sequence from Figure 18. b) Four-quantum-filtered spectrum obtained with the pulse sequence from Figure 18. c) C_4 spin-topology-filtered spectrum obtained with the pulse sequence from Figure 19 (from ref. 94).

Scheme 1. The interpretation is left to the reader. Only cross peaks of the molecule with K_4 topology and diagonal peaks of molecules with $P_{3,1}$, S_4, and K_4 topologies remain.

Technically, multiple-quantum filtering exploits the characteristic dependence of a multiple-quantum coherence transfer on the rf phase of the acting pulse sequence (8,92,95,96). Let us assume a transfer of coherence $c_{p1}(t)$ by a unitary transformation $\mathbf{U}(0)$, representing a particular pulse sequence, to coherence $c_{p2}(t)$, where p_1 and p_2 are the orders of coherence.

$$c_{p1}(t) \xrightarrow{\mathbf{U}(0)} c_{p2}(t) \tag{14}$$

All rf pulses in the sequence are now phase-shifted by Φ, leading to $\mathbf{U}(\Phi)$. Then it can be shown that the resulting coherence $c_{p2}(t)$ is phase-shifted by $(p_2 - p_1)\Phi$.

$$c_{p1}(t) \xrightarrow{\mathbf{U}(\Phi)} c_{p2}(t)e^{i(p2-p1)\Phi} \tag{15}$$

The phase shift is therefore proportional to the change in coherence order ($\Delta p = p_2 - p_1$). After a series of experiments are performed in which the phase

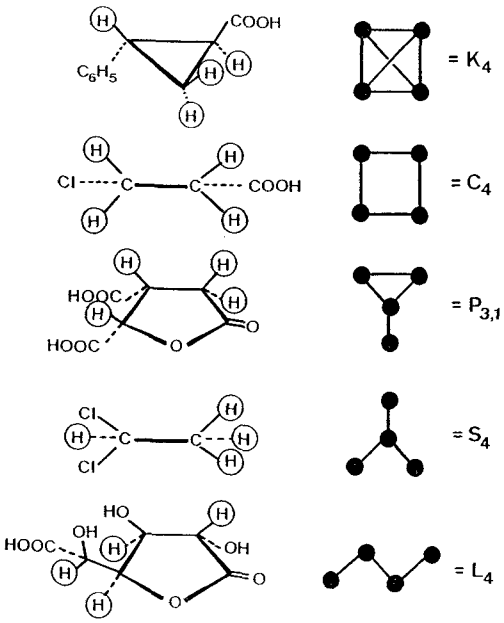

Scheme 1. The compounds used for the spectra in Figure 17 and their spin-coupling topologies.

Φ is incremented in regular intervals $2\pi/N$ from 0 to $2\pi(N-1)/N$, it is possible to select for a particular Δp by computing the corresponding Fourier coefficient of Δp: Let $s(t,\Phi)$ be the recorded signal of an experiment with phase shift Φ, then we obtain the filtered signal according to eqn. 16.

$$s(t,\Delta p) = \sum_{k=0}^{N-1} s(t, 2\pi k/N) \mathrm{e}^{-\mathrm{i}2\pi k \Delta p/N} \qquad (16)$$

The required number of increments N of the phase Φ depends on the number of values of Δp that have to be discriminated (96). It is obvious that unless the initial order of coherence p_1 is known, no particular order of coherence p_2 can be filtered out in this manner. Most conveniently the initial state is selected to be in thermal equilibrium with $p_1 = 0$. Then, the entire pulse sequence preceding the point at which a coherence order should be selected must be phase-cycled. For multiple-quantum-filtered COSY experiments, this leads to the pulse sequence shown in Figure 18.

Obviously, multiple-quantum-filtering and phase cycling require N-times more experiments. However, no information is lost, since in each term of eqn. 16 just the phase factor is compensated, and identical signals are coadded for the relevant pathways. Thus the longer performance time is refunded in terms of an increased signal-to-noise ratio.

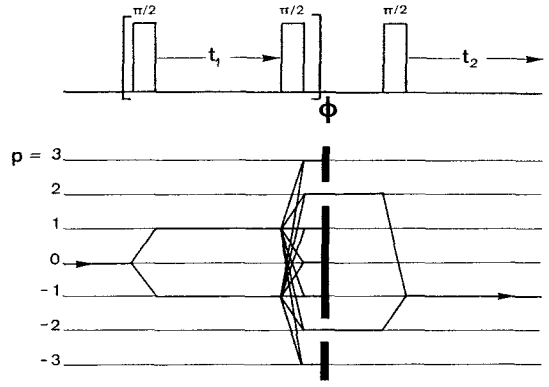

Figure 18: Pulse sequence for multiple-quantum-filtered COSY experiment with the coherence transfer diagram for double-quantum filtering. The phase ϕ is incremented systematically in a set of N experiments and the resulting experimental results are combined according to eqn. 16.

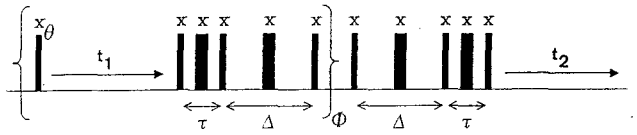

Figure 19: Pulse sequence for C_4 spin-topology filtration consisting of $\pi/2$ and π pulses. The delays are adjusted to $\tau = 1/(8J)$ and $\Delta = 1/(2J)$, where J is the uniform J-coupling constant. ϕ is phase-cycled for four-quantum selection and θ for the suppression of axial peaks (94).

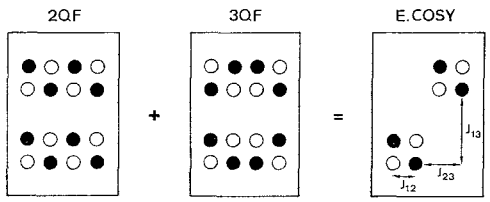

Figure 20: E. COSY experiment to simplify the multiplet structure of cross peaks. The double-quantum- and the triple-quantum-filtered cross peak between spins I_1 and I_2 of a three-spin system are combined to produce an E. COSY pattern. Positive and negative multiplet components are distinguished by empty and filled circles.

IX. Spin-Topology Filtration

It may be desirable to enhance the filtering effect illustrated in Figure 17 and to select individual spin coupling topologies. Indeed it is possible to design extended pulse sequences, in combination with multiple-quantum filtration, that are tailor-made for specific spin coupling topologies (94,97,98). A pulse sequence built into a 2D COSY experiment, that is selective for cyclic C_4 spin coupling topologies is depicted schematically in Figure 19. If this pulse sequence is applied to the mixture of compounds with four-spin systems (Scheme 1), the 2D spectrum of Figure 17c is obtained. It shows efficient suppression of all other spin systems. It should be noted, however, that the situation is here rather ideal. Often, these filters do not perform as well because their design relies on all non-zero spin couplings being equal. In reality, there are weak and strong couplings that cannot be characterized by topological considerations alone. Often also the intensities of signals decrease during the extended pulse sequences due to relaxation. This limits the practical usefulness of these methods.

X. Exclusive Correlation Spectroscopy

Multiple-quantum filtering suppresses not only diagonal and cross peaks in 2D spectra but also changes the sign pattern in the cross-peak multiplet structure. By appropriate combination of differently multiple-quantum-filtered 2D spectra, it is possible to simplify the multiplet structure by reducing the number of multiplet components. Exclusive correlation spectroscopy (E. COSY), proposed by O.W. Sørensen, eliminates all multiplet components from a COSY spectrum except for those belonging to pairs of transitions with an energy level in common (99-101). In practice, it is not necessary to combine multiple-quantum-filtered spectra literally, but it is possible to coadd directly the experimental results from a phase cycle with the appropriate weighting factors.

Figure 20 shows schematically the combination of cross-peak multiplets connecting two spins, I_1 and I_2, in a three-spin system after double- and triple-quantum filtering. The remaining pattern consists of two basic squares with side lengths equal to the active coupling constant J_{12} responsible for the coherence transfer. The displacement vector between the two squares is given by the two passive couplings J_{13} and J_{23} to the third (passive) spin. It should be mentioned that this multiplet structure is identical to the one obtained by a COSY experiment with a mixing pulse with an extremely small flip angle (102).

E. COSY is of practical use whenever the cross-peak multiplet structure must be analyzed for the determination of J-coupling constants. This can be done conveniently by hand by measuring the displacement of peripheral multiplet components (101) or by a recursive contraction procedure on a computer (103).

XI. Heteronuclear Two-Dimensional Experiments

In addition to the homonuclear 2D experiments discussed so far, at least as many heteronuclear experiments have been proposed and introduced to the repertoire of routine spectroscopy methods. Of greatest practical importance are heteronuclear shift correlation spectra which correlate the chemical shifts of directly bonded or remotely connected heteronuclei (104,105). In this context, so-called inverse detection experiments are of particular interest. Here proton I-spin coherence is observed in t_2 while spin coherence of a less sensitive, less abundant S nucleus evolves in t_1 (104). The most efficient pulse sequences create heteronuclear two-spin coherence that evolves in t_1 and that acquires the frequency information of the S-spin resonance (106). Also in the heteronuclear environment, relayed coherence transfer (78) as well as experiments in the rotating frame (107) are important. Spin filtering is used for multiplicity selectivity, that is, for distinguishing S spins coupled to one, two, or three I spins (108), and in the form of J filtering for the distinction of one-bond and multiple-bond couplings (109). This enumeration of heteronuclear experiments is by no means exhaustive.

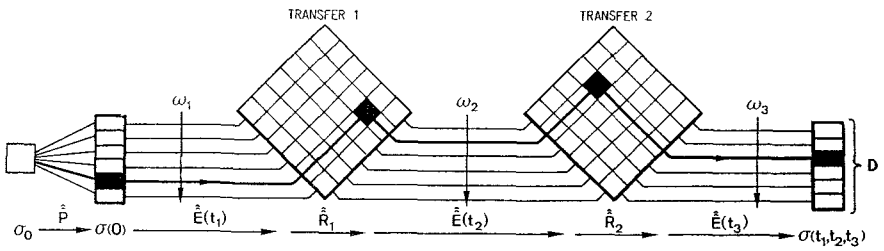

Figure 21: Schematic representation of a 3D NMR experiment as an extension of Figures 1 and 6. Three evolution periods with the time variables t_1, t_2, and t_3 are separated by two transfer or mixing processes with the transfer matrices R1 and R2. A 3D experiment can be conceived as the contraction of two 2D experiments.

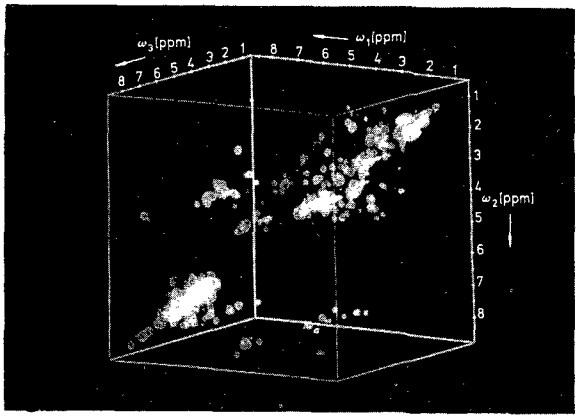

Figure 22: 3D representation of a 300 MHz 3D homonuclear ROESY-TOCSY spectrum of buserilin in [D_6]DMSO photographed from a computer screen (116).

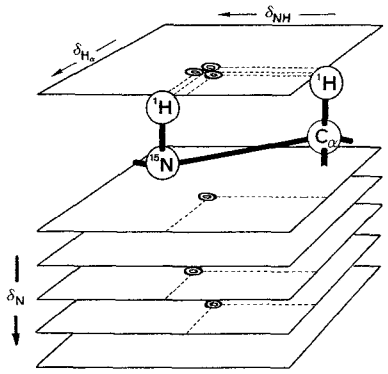

Figure 23: 3D resolution of a 2D ^{1}H NMR spectrum by ^{15}N resonance spreading. The NH–C_αH cross peaks are displaced in a third dimension by the corresponding ^{15}N chemical shifts.

XII. Three-Dimensional Fourier-Transformation Spectroscopy

No new principles are required for the development of 3D NMR spectroscopy, which is just a logical extension of 2D NMR spectroscopy. Instead of a single mixing process which relates two frequency variables, two sequential mixing processes relate three frequencies: the origin frequency ω_1, the relay frequency ω_2, and the detection frequency ω_3 (Figure 21). In this sense a 3D experiment can be considered as the combination of two 2D experiments. Obviously a very large number of possible 3D experiments can be conceived. However, only few of them have proved to be indispensible so far (110-118).

Two applications of the 3D spectroscopy concept have emerged: 1) 3D correlation and 2) 3D dispersion spectroscopy (see also Fig. 13). Three-dimensional correlation is of importance in homonuclear experiments. It has been mentioned that the assignment procedure in biomolecules requires a COSY-type and a NOESY-type 2D spectrum. The two 2D experiments could be contracted into one 3D experiment, combining a J-coupling-mediated transfer and a cross-relaxation transfer. A 3D COSY–NOESY spectrum possesses the advantage that the entire assignment process can be carried out with a single homogeneous data set (115,116). It also incorporates redundant information that allows cross checks of the assignments. For obtaining quantitative information, however, 3D spectra are less suited, since all peak intensities are products of

two transfer coefficients that are sometimes difficult to separate.

A 3D ROESY–TOCSY spectrum of the linear nonapeptide buserilin is shown in Figure 22 (vf. Fig. 14)(116). A ROESY instead of a NOESY sequence is required for buserilin, as it is a molecule of intermediate size for which the NOE intensities are small. The TOCSY step has the advantage that chains of multiple-step cross peaks extend to nuclei in the side chains are obtained thus facilitating the identification of the amino acid residues.

It should be recognized that recording a 3D spectrum is considerably more time-consuming than two 2D spectra, since two time parameters, t_1 and t_2, must be incremented independently, requiring a 2D array of experiments. Thus the question arises of when it is worth the effort to record a 3D spectrum. This question has been discussed in numerous publications (116,119,120).

Let us consider a particular cross peak in a 3D spectrum that correlates the coherences $\{tu\}$ in the ω_1, $\{rs\}$ in the ω_2 and $\{pq\}$ in the ω_3 dimension. Its intensity is determined by the following product (eqn. 17) of matrix elements in the eigenbasis of the unperturbed Hamiltonian $\mathcal{H}_0$ (116).

$$Z_{\{pq\}\{rs\}\{tu\}} = D_{qp} R^{(2)}_{\{pq\}\{rs\}} R^{(1)}_{\{rs\}\{tu\}} (\hat{\hat{\mathrm{P}}}\sigma_0)_{tu} \quad (17)$$

A nonvanishing intensity establishes a two-step correlation $\{tu\}$–$\{rs\}$–$\{pq\}$.

The 3D experiment can be compared with two 2D experiments that employ the mixing processes $\hat{\hat{\mathrm{R}}}^{(1)}$ and $\hat{\hat{\mathrm{R}}}^{(2)}$, respectively. The corresponding intensities are expressed by eqns. 18 and 19.

$$Z^{(1)}_{\{rs\}\{tu\}} = D^{(1)}_{sr} R^{(1)}_{\{rs\}\{tu\}} (\hat{\hat{\mathrm{P}}}\boldsymbol{\sigma}_0)_{tu} \quad (18)$$

$$Z^{(2)}_{\{pq\}\{rs\}} = D_{qp} R^{(2)}_{\{pq\}\{rs\}} (\hat{\hat{\mathrm{P}}}^{(2)}\boldsymbol{\sigma}_0)_{rs} \quad (19)$$

If in the 2D spectra the two relevant peaks with intensities $\mathrm{Z}^{(1)}_{\{rs\}\{tu\}}$ and $\mathrm{Z}^{(2)}_{\{pq\}\{rs\}}$ can be identified, possibly in crowded regions, the two-step correlation, represented by a 3D peak, could also be established based on the two 2D spectra $\{tu\}$–$\{rs\}$ and $\{rs\}$–$\{pq\}$. Provided that $Z_{\{pq\}\{rs\}\{tu\}} \neq 0$ is true, the intensities $Z^{(1)}_{\{rs\}\{tu\}}$ and $Z^{(2)}_{\{pq\}\{rs\}}$ are different from zero when in addition $D^{(1)}_{sr} \neq 0$ and $(\hat{\hat{\mathrm{P}}}^{(2)}\boldsymbol{\sigma}_0)_{rs} \neq 0$ hold. This implies that the relay transition $\{rs\}$ must be excited in the preparation state $P^{(2)}$ and detectable by the observable $D^{(1)}$. For allowed one-spin single-quantum coherences, this condition is fulfilled for single-pulse excitation and direct detection. On the other hand, forbidden multiple-spin single-quantum coherences (combination lines) and multiple-quantum coherences can neither be excited by a single nonselective pulse nor directly detected. Such coherences regularly occur in the ω_2 dimension of a 3D spectrum. The excitation and indirect detection of these coherences in 2D experiments requires special pulse sequences for excitation and detection.

In conclusion, the two constituent 2D experiments deliver the same information on the spin system as the 3D spectrum, provided that 1) the relevant frequencies in the ω_2 dimension of the 3D spectrum can be excited and detected in the 2D experiments, and 2) the cross peaks are not hidden by spectral overlap and can be identified in the 2D spectra. The first condition is normally not severe, as the 2D experiments can be modified for excitation and detection of forbidden transitions whenever required. On the other hand, the limited resolving power of 2D spectra is the most important motivation for justifying 3D (and possibly higher dimensional) spectroscopy.

Because the gain in resolution justifies 3D spectroscopy, it may be worthwhile to introduce a third frequency axis just for resolution purposes, rather than combining two processes relevant for the assignment requiring high resolution in all three dimensions. It is then possible to choose the extent of 3D resolution arbitrarily and optimize the performance time of the 3D experiment. To spread a 2D spectrum into a third dimension, homonuclear or heteronuclear transfers can be used. Heteronuclear one-bond transfers are far more efficient, however, because the strong heteronuclear one-bond couplings prevent leakage to further spins. This allows an efficient transfer, virtually without loss of magnetization. In addition, nuclei like ^{13}C and ^{15}N exhibit large ranges of chemical shifts with high resolving power. The principle of spreading is represented graphically in Figure 23.

A 3D ^{15}N-spread TOCSY spectrum of ribonuclease A is shown in Figure 24. Heteronuclear spreading requires usually isotopic labeling of the molecule.

In this case, ribonuclease A was grown in an *E. coli* medium containing ^{15}N-labeled nutrients. The spectrum was obtained with the pulse sequence from Figure 25. Initially proton coherence is excited and precesses during t_1 under ^{15}N refocusing by the applied π pulse. During the mixing time τ_m, coherence transfer from other protons to the NH protons is effected in the rotating frame by the application of a TOCSY multiple-pulse sequence. The NH coherence is then converted into ^{15}NH heteronuclear multiple-quantum coherence (HMQC) which precesses during t_2 and acquires ^{15}N resonance information (under proton refocusing). After reconversion into NH proton coherence, detection follows during t_3 under ^{15}N decoupling. For a complete assignment of the proton resonances a ^{15}N-spread NOESY spectrum is required in addition.

The step to 4D spectroscopy (121) is a logical one: In 2D experiments, spins are pairwise correlated, for example NH and C_αH protons. Three-dimensional dispersion uses either ^{15}N or $^{13}C_\alpha$ resonance for spreading the resonances of NH or C_αH, respectively. In a 4D experiment, both spreading processes are applied simultaneously (Scheme 2). The order of the frequencies in the actual experiment is a matter of convenience. Normally, the detection frequency ω_4 refers to proton spins for sensitivity reasons. In most cases, the two spreading coordinates are rather coarsely digitized to limit the performance time, just enough to achieve separation of peaks overlapping in the 2D spectrum. Often 8 to 32 points in each of the two dimensions are sufficient.

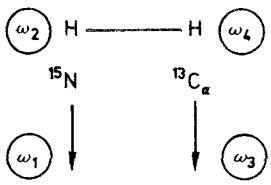

Scheme 2. Double spreading in 4D experiments.

XIII. Molecular Dynamics Investigated by NMR

The molecular structures determined by NMR spectroscopy in solution, by X-ray diffraction in single crystals, or by other means are invariably motionally averaged structures, whereby the averaging

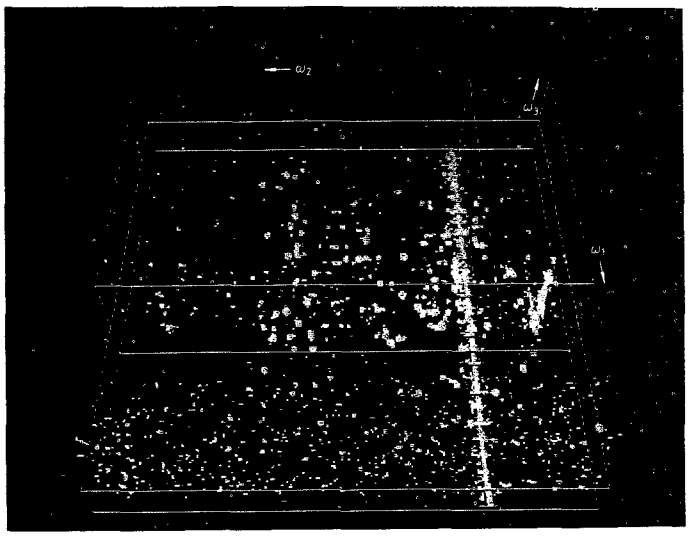

Figure 24: 3D ^{15}N-spread 600 MHz ^{1}H TOCSY spectrum of ^{15}N-labeled ribonuclease A in water. The 3D spectrum shows the ^{15}N resonances along the ω_2 axis. The spectrum was recorded by C. Griesinger with the pulse sequence from Figure 25 and processed by S. Boentges. The sample was provided by Prof. S. Benner of ETH Zurich.

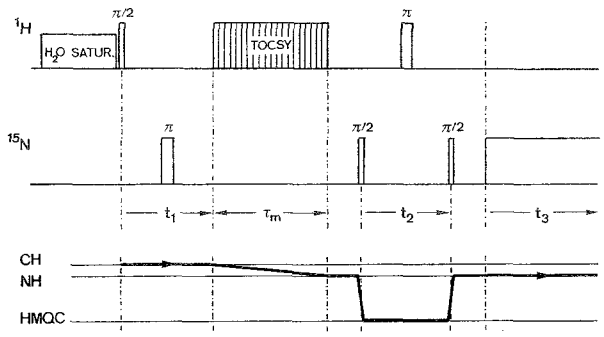

Figure 25: Pulse sequence for recording a 3D ^{15}N-spread TOCSY spectrum. After presaturation of the water resonance (I), the proton resonances are excited and precess during t_1. After the homonuclear TOCSY transfer from CH to the NH protons, the coherence is converted into heteronuclear multiple-quantum coherence (HMQC) that evolves during t_2 and acquires ^{15}N shift information. After reconversion to proton coherence, the NH resonances are detected during t_3 under ^{15}N decoupling.

process is strongly dependent on the measurement technique. To interpret experimentally determined structures, some knowledge of the motional properties of the molecule is in fact indispensible. Molecular dynamics is also relevant for its own sake, in particular for the understanding of reactivity and interaction with other molecules. In many cases, active sites in a molecular pocket are only accessible due to the flexibility of the molecule itself.

The characterization of the motional properties of a molecule is orders of magnitude more difficult than the description of an averaged molecular structure. While $3N$–6 coordinates are sufficient to fix a structure containing N atoms, the characterization of molecular dynamics requires $3N$–6 variances of the intramolecular coordinates, $(3N–6)(3N–5)/2$ covariances, and the same number of auto- and cross-correlation functions, respectively. In addition, also higher order correlation functions are needed for a more refined description of dynamics. In practice, a sufficient number of observables is never available for a full description of dynamics. In this sense, the study of dynamics is an open-ended problem.

Numerous techniques are available for obtaining data on dynamics: Debye-Waller factors in X-ray diffraction give hints on the variances of the nuclear coordinates, however, without a measure for the time scale. Inelastic and quasielastic neutron scattering deliver correlation functions, but without a reference to the structure. Fluorescence depolarization allows one to determine the motional correlation function of fluorescent groups, such as tyrosine residues in proteins. Ultrasonic absorption gives an indication of the frequencies of the dominant motional modes, but again without a structural reference.

NMR spectroscopy is more universally applicable to motional studies than most of the other techniques. The range of correlation times τ_c that can be covered by various NMR methods is enormous, from picoseconds to seconds and more (Scheme 3).

$1\ \text{s} < \tau_c$:	Real-time monitoring after initial perturbation
$10\ \text{ms} < \tau_c < 10\ \text{s}$:	2D exchange spectroscopy (EXSY)
$100\ \mu\text{s} < \tau_c < 1\ \text{s}$:	Lineshape analysis, exchange broadening, and exchange narrowing
$1\ \mu\text{s} < \tau_c < 10\ \text{ms}$:	Measurements of relaxation time $T_{1\varrho}$ in the rotating frame
$30\ \text{ps} < \tau_c < 1\mu\text{s}$:	Measurements of relaxation time T_1 in the laboratory frame
$\tau_c < 100\ \text{ps}$:	Averaged parameter values

Scheme 3. NMR methods for the determination of motional correlation times τ_c

Except for slow motions on a time scale of a millisecond or more for which lineshape analysis, saturation transfer experiments, and 2D exchange studies can be performed, many dynamics studies by NMR rely on measurements of relaxation times. The various relaxation parameters, such as the longitudinal relaxation time T_1, the transverse relaxation time T_2, the rotating-frame relaxation time $T_{1\varrho}$, and cross-relaxation rate constants Γ_{kl} depend on the correlation time τ_c of the underlying random process.

The following discussion shall be restricted to a recent study of the intramolecular dynamics in antamanide (**1**) (83,122,123) (see Figs. 8,9,11). Antamanide is an antidote for toxic components of the mushroom *Amanita phalloides*. Astonishingly, the antidote is a component of the same mushroom. Indications have been found in early ultrasonic absorption studies (124) that the peptide ring seems to undergo a conformational exchange process with a frequency of about 1 MHz. In the course of extensive investigations of antamanide by Kessler's research group (125), it has also been noticed that the distance constraints obtained from NMR measurements could not be fitted by a single conformation. In our laboratory Martin Blackledge performed rotating-frame relaxation measurements and localized a hydrogen-bond exchange process with an activation energy of about 20 kJ mol^{-1} and a lifetime of 25 μs at room temperature (unpublished results, see also ref. 126). With a new dynamic structure determination procedure called MEDUSA (123), the conformational space of antamanide was investigated more systematically than ever before. 1176 feasible low-energy structures were found. They were combined in dynamically

interconverting pairs in an attempt to fulfill all experimental constraints including NOE distance constraints, *J*-coupling angular constraints, and specific information on hydrogen-bond dynamics. A large set of feasible structural pairs were constructed. Many pairs are compatible with the experimental data within experimental accuracy. For a more restrictive description of the dynamic system of antamanide, additional and more accurate experimental data is required. Figure 26 shows, as an example, the dynamic pair of structures that fits the experimental data best so far. The two interconverting structures differ primarily in the hydrogen bonds Val^{1}NH–Phe^{9}O and Phe^{6}NH–Ala^{4}O, which exist only in one of the two conformations (**II**), and in the torsional angles ϕ_5 and ϕ_{10}.

A second study concentrated on the dynamics of ring puckering of the four proline residues in antamanide (122). The conformation of the five-ring systems can be determined from the dihedral angles χ_1, χ_2, and χ_3 which in turn can be deduced from the vicinal proton–proton *J*-coupling constants using the Karplus relations (54). The relevant coupling constants (21 per residue) were determined from E. COSY spectra. Based on these measurements, a model was constructed for each of the proline residues by least-squares fitting. It was found that for Pro^3 and Pro^8 a good fit can be obtained with a single rigid conformation, while for Pro^2 and Pro^7 two rapidly exchanging conformations were required to reduce the fitting error to within an acceptable range. At the same time, measurements of the ^{13}C relaxation time confirmed that Pro^3 and Pro^8 are rigid, while Pro^2 and Pro^7 show dynamic behavior with correlation times between 30 and 40 ps. This implies that the dynamics of the peptide ring and the proline ring are not correlated and proceed on entirely different time scales. The two exchanging conformations found for Pro^2 are shown in Figure 27. It is seen that the conformational changes resemble the up and down movements of the "flap of the envelope" (C_γ).

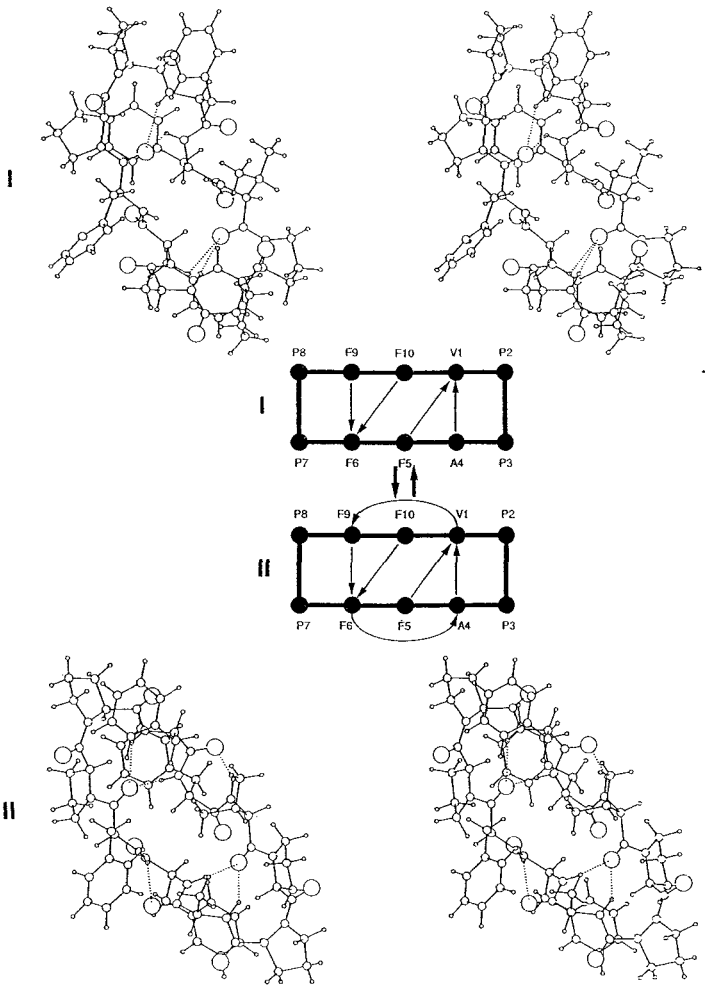

Figure 26: Pairs of conformers of antamanide that fulfill the experimentally determined structural constraints. The two pairs are shown as stereoplots as well as in abstract form. In the former, hydrogen bonds are indicated by broken lines, in the latter by arrows pointing towards the hydrogen-bonded oxygen atom. The C–C$_\alpha$ bonds about which the torsion angles ϕ_5 and ϕ_6 are defined are indicated by heavy lines. ϕ_5 is in the lower and ϕ_{10} in the upper half of the stereoplots. (from ref. 123).

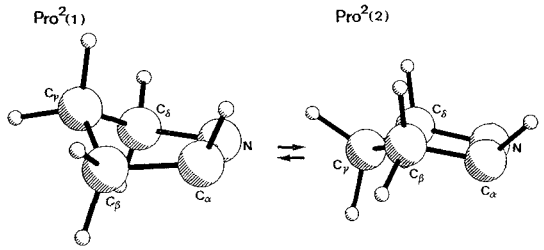

Figure 27: The two experimentally determined conformations of the amino acid residue Pro^2 in antamanide (**1**) (see ref. 122).

XIV. Magnetic Resonance Fourier Imaging

Magnetic resonance imaging (MRI) has had an enormous impact on medical diagnosis and has rapidly become a powerful routine tool. The basic

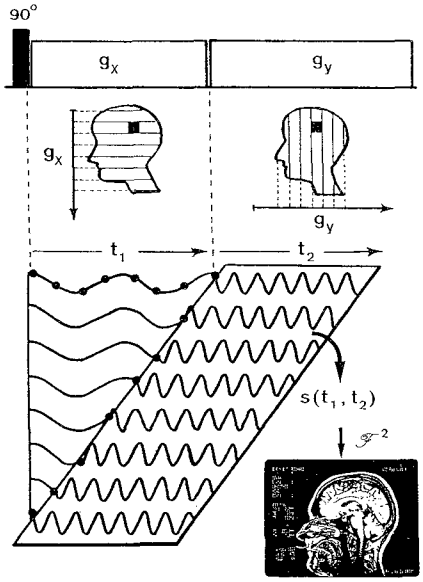

Figure 28: Schematic representation of Fourier NMR imaging, here shown in two dimensions. Two orthogonal gradients (g_x, g_y) are applied during the t_1 and t_2 periods of a 2D experiment. A 2D Fourier transformation of the data set $s(t_1, t_2)$ produces a 2D image of the investigated subject (R.R.E.).

procedure for recording a 2D or 3D NMR image of an object is attributed to Paul Lauterbur (127). A magnetic field gradient, applied along different directions in space in a sequence of experiments, produces projections of the nuclear spin density of the object onto the direction of the gradient. From a sufficiently large set of such projections it is possible to reconstruct an image of the object, for example, by filtered backprojection in analogy to X-ray tomography.

A different approach is directly related to 2D and 3D FT spectroscopy. Frequency encoding of the three spatial dimensions is achieved by a linear magnetic field gradient applied successively along three orthogonal directions for the durations t_1, t_2, and t_3, respectively, in a pulse FT experiment (128). In full analogy to 3D spectroscopy, the time parameters t_1 and t_2 are incremented in regular intervals from experiment to experiment. The recorded signal $s(t_1, t_2, t_3)$ is Fourier-transformed in three dimensions to produce a function $S(\omega_1, \omega_2, \omega_3)$ which is equivalent to a 3D spatial image when the spatial information is decoded using the relations $x = \omega_1/g_x, y = \omega_2/g_y$, and $z = \omega_3/g_z$ with the three field gradients g_x, g_y, and g_z. The procedure is illustrated in Figure 28 for two dimensions.

In a further refinement, proposed by Edelstein et al. (129), the time variables t_1 and t_2 are replaced by variable field gradient strengths g_x and g_y applied during a constant evolution time. With regard to the accumulated phase, (eqn. 20) it is immaterial whether the evolution time or the field gradients are varied.

$$\gamma = x g_x t_1 + y g_y t_2 + z g_z t_3 \qquad (20)$$

However, keeping the time t_k constant eliminates undesired relaxation effects.

In medical imaging, 3D experiments have a natural justification, although it is sometimes simpler to apply selective excitation techniques to select a 2D slice through the object to be imaged (130). Even extensions to higher dimensions are quite realistic. In a fourth dimension, for example, chemical shift information can be accommodated (131). Also 2D spectroscopic information could be combined with three spatial dimensions, leading to a 5D experiment. No limitations seem to exist for human imagination. However, the practical limits will soon be reached when the required performance times are also taken into consideration.

XV. Conclusion

I am not aware of any other field of science outside of magnetic resonance that offers so much freedom and opportunities for a creative mind to invent and explore new experimental schemes that can be fruitfully applied in a variety of disciplines. NMR spectroscopy is intellectually attractive because the observed phenomena can be understood based on a sound theory, and almost all conceits can also be tested by easy experiments. At the same time, the practical importance of NMR is enormous and can justify much of the playful activities of an addicted spectroscopist.

Most of the credit for the inspiration and execution of the work described should go to my teachers Hans Primas and Hans H. Günthard, to my supervisor Weston A. Anderson, to the inspirator Jean Jeener, and to my co-workers (in more or less chronological order): Thomas Baumann, Enrico Bartholdi, Robert Morgan, Stefan Schäublin, Anil Kumar, Dieter Welti, Luciano Müller, Alexander

Wokaun, Walter P. Aue, Jiri Karhan, Peter Bachmann, Geoffrey Bodenhausen, Peter Brunner, Alfred Höhener, Andrew A. Maudsley, Kuniaki Nagayama, Max Linder, Michael Reinhold, Ronald Haberkorn, Thierry Schaffhauser, Douglas Burum, Federico Graf, Yongren Huang, Slobodan Macura, Beat H. Meier, Dieter Suter, Pablo Caravatti, Ole W. Sørensen, Lukas Braunschweiler, Malcolm H. Levitt, Rolf Meyer, Mark Rance, Arthur Schweiger, Michael H. Frey, Beat U. Meier, Marcel Müri, Christopher Councell, Herbert Kogler, Roland Kreis, Norbert Müller, Annalisa Pastore, Christian Schönenberger, Walter Studer, Christian Radloff, Albert Thomas, Rafael Brüschweiler, Herman Cho, Claudius Gemperle, Christian Griesinger, Zoltan L. Mádi, Peter Meier, Serge Boentges, Marc McCoy, Armin Stöckli, Gabriele Aebli, Martin Blackledge, Jacques Briand, Matthias Ernst, Tilo Levante, Pierre Robyr, Thomas Schulte-Herbrüggen, Jürgen Schmidt and Scott Smith. I would also like to thank my technical staff, Hansruedi Hager, Alexandra Frei, Janos A. Deli, Jean-Pierre Michot, Robert Ritz, Thomas Schneider, Markus Hintermann, Gerhard Gucher, Josef Eisenegger, Walter Lämmler and Martin Neukomm; my secretary Irène Müller; and several research groups with which I had the pleasure to collaborate, first of all the research group of Kurt Wüthrich and the group of Horst Kessler. I am grateful for support in the early days from Varian Associates and more recently from the Swiss Federal Institute of Technology, the Swiss National Science Foundation, the Kommission zur Förderung der Wissenschaftlichen Forschung, and last but not least to Spectrospin AG.

XVI. References

[1]I.I. Rabi, *Phys. Rev.* **51**, 652 (1937).

[2]I.I. Rabi, J.R. Zacharias, S. Millman, and P. Kusch, *Phys. Rev.* **53**, 318 (1938); I.I. Rabi, S. Millman, P. Kusch, and J.R. Zacharias, *ibid.* **55**, 526 (1939).

[3]J.M.B. Kellogg, I.I. Rabi, N.F. Ramsey, and J.R. Zacharias, *Phys. Rev.* **55**, 318 (1939); *ibid.* **56**, 728 (1939); *ibid.* **57**, 677 (1940).

[4]E.M. Purcell, H.G. Torrey, and R.V. Pound, *Phys. Rev.* **69**, 37 (1946).

[5]F. Bloch, W. Hansen, and M.E. Packard, *Phys. Rev.* **69**, 127 (1946).

[6]F. Bloch, *Phys. Rev.* **70**, 460 (1946).

[7]J. Brossel and A. Kastler, *C. R. Hebd. Seances Acad. Sci.* **229**, 1213 (1949); A. Kastler, *J. Phys. Radium* **11**, 255 (1950).

[8]R.R. Ernst, G. Bodenhausen, and A. Wokaun, "Principles of NMR in One and Two Dimensions", Clarendon Press, Oxford, 1987.

[9]A. Bax, "Two-Dimensional NMR in Liquids", Delft University Press, Reidel, Dortrecht, 1982.

[10]Attur-ur Rahman, "Nuclear Magnetic Resonance, Basic Principles", Springer, New York, 1986.

[11]N. Chandrakumar and S. Subramanian, "Modern Techniques in High-Resolution FT-NMR", Springer, New York, 1987.

[12]H. Friebolin, "Ein- und zweidimensionale NMR-Spektroskopie", VCH, Weinheim, 1988; "Basic One- and Two-Dimensional NMR Spectroscopy", VCH, Weinheim, 1991.

[13]G.E. Martin and A.S. Zektzer, "Two-Dimensional NMR Methods for Establishing Molecular Connectivity", VCH, Weinheim, 1988.

[14]J. Schraml and J.M. Bellama, "Two-Dimensional NMR Spectroscopy", Wiley Interscience, New York, 1988.

[15]"Pulse Methods in 1D and 2D Liquid-Phase NMR", (Ed.: W.S. Brey), Academic Press, New York, 1988.

[16]A.A. Michelson, *Philos. Mag. Ser. 5*, **31**, 256 (1981); A.A. Michelson, "Light Waves and Their Uses", University of Chicago Press, Chicago, 1902.

[17]P. Fellgett, Dissertation, Cambridge University, 1951; P. Fellgett, *J. Phys. Radium* **19**, 187 (1958).

[18]*Varian Associates Magazine*, **24**, (7), 11 (1979); *IEEE Center for the History of Electrical Engineering Newsletter* (24), 2 (1990).

[19]R.R. Ernst and W.A. Anderson, *Rev. Sci. Instrum.* **37**, 93 (1966).

[20]R.R. Ernst, *Adv. Magn. Reson.* **2**, 1 (1966).

[21]W.A. Anderson and R.R. Ernst, US-A 3 475 680 (Impulse Resonance Spectrometer Including a Time Averaging Computer and a Fourier Analyzer), 1969 (submitted May 26, 1965).

[22]R.R. Ernst, in "The Applications of Computer Techniques in Chemical Research", The Institute of Petroleum, London, 1972, p.61.

[23]O.W. Sørensen, G.W. Eich, M.H. Levitt, G. Bodenhausen, and R.R. Ernst, *Prog. Nucl. Magn. Reson. Spectrosc.* **16**, 163 (1983).

[24]J.B.J. Fourier, "Theorie analytique de la chaleur", Firmin Didot, Père et fils, Paris, 1822.

[25]I.J. Lowe and R.E. Norberg, *Phys. Rev.* **107**, 46 (1957).

[26]N. Wiener, *Mass. Inst. Technol. Res. Lab. Radiation Rep.*, (V) 16 S (1942); "Nonlinear Problems in Random Theory", Wiley, New York, 1958.

[27]R.H. Varian, US-A 3 287 629 (Gyromagnetic Resonance Methods and Apparatus), 1966 (submitted August 29, 1956).

[28]H. Primas, *Helv. Phys. Acta* **34**, 36 (1961).

[29]R.R. Ernst and H. Primas, *Helv. Phys. Acta* **36**, 583 (1963).

[30]R.R. Ernst, *J. Chem. Phys.* **45**, 3845 (1966).

[31]R.R. Ernst, *Mol. Phys.* **16**, 241 (1969).

[32]R. Kaiser, *J. Magn. Reson.* **3**, 28 (1970).

[33]R.R. Ernst, *J. Magn. Reson.* **3**, 10 (1970).

[34]D. Ziessow and B. Blümich, *Ber. Bunsenges. Phys. Chem.* **78**, 1169 (1974); B. Blümich and D. Ziessow, *J. Chem. Phys.* **78**, 1059 (1983).

[35]B. Blumich, *Bull. Magn. Reson.* **7**, 5 (1985).

[36]J. Dadok and R.F. Sprecher, *J. Magn. Reson.* **13**, 243 (1974).

[37]R.K. Gupta, J.A. Ferretti, and E.D. Becker, *J. Magn. Reson.* **13**, 275 (1974).

[38]J.A. Ferretti and R.R. Ernst, *J. Chem. Phys.* **65**, 4283 (1976).

[39]B.L. Tomlinson and H.D.W. Hill, *J. Chem. Phys.* **59**, 1775 (1973).

[40]M.H. Levitt and R. Freeman, *J. Magn. Reson.* **33**, 473 (1979).

[41]M.H. Levitt, *Prog. Nucl. Magn. Reson. Spectrosc.* **18**, 61 (1986).

[42]R.L. Vold, J.S. Waugh, M.P. Klein, and D.E. Phelps, *J. Chem. Phys.* **48**, 3831 (1968).

[43]R. Freeman and H.D.W. Hill, in "Dynamic NMR Spectroscopy" (Eds.: L.M. Jackman and F.A. Cotton), Academic Press, New York, 1975, S.131.

[44]S. Forsén and R.A. Hoffman, *J. Chem. Phys.* **39**, 2892 (1963).

[45]H.C. Torrey, *Phys. Rev.* **75**, 1326 (1949); *ibid.* **76**, 1059 (1949).

[46]E.L. Hahn, *Phys. Rev.* **76**, 145 (1949).

[47]E.L. Hahn, *Phys. Rev.* **80**, 297 (1950).

[48]E.L. Hahn, *Phys. Rev.* **80**, 580 (1950).

[49]M. Emshwiller, E.L. Hahn, and D. Kaplan, *Phys. Rev.* **118**, 414 (1960).

[50]S.R. Hartmann and E.L. Hahn, *Phys. Rev.* **128**, 2042 (1962).

[51]M.B. Comisarow and A.G. Marshall, *Chem. Phys. Lett.* **25**, 282 (1974); *ibid.* **26**, 489 (1974).

[52]J.C. McGurk, H. Mäder, R.T. Hofmann, T.G. Schmalz, and W.H. Flygare, *J. Chem. Phys.* **61**, 3759 (1974).

[53]For example, M.K. Bowman in "Modern Pulsed and Continuous-Wave Electron Spin Resonance", (Eds.: L. Kevan, M.K. Bowman), J. Wiley, New York, 1990, p.1.

[54]M. Karplus, *J. Chem. Phys.* **30**, 11 (1959).

[55]J.H. Noggle and R.E. Schirmer, "The Nuclear Overhauser Effect", Academic Press, New York, 1971.

[56]K. Wüthrich, "NMR of Proteins and Nucleic Acids", Wiley Interscience, New York, 1986.

[57]S. Yatsiv, *Phys. Rev.* **113**, 1522 (1952).

[58]W.A. Anderson and R. Freeman, *J. Chem. Phys.* **37**, 85 (1962).

[59]R. Freeman and W.A. Anderson, *J. Chem. Phys.* **37**, 2053 (1962).

[60]R.A. Hoffman and S. Forsén, *Prog. Nucl. Magn. Reson. Spectrsoc.* **1**, 15 (1966).

[61]J. Jeener, *Ampère International Summer School* (Basko Polje, Yugoslavia) 1971, unpublished.

[62]R.R. Ernst, *VIth International Conference on Magnetic Resonance in Biological Systems* (Kandersteg, Switzerland) 1974, unpublished.

[63]W.P. Aue, E. Bartholdi, and R.R. Ernst, *J. Chem. Phys.* **64**, 2229 (1976).

[64]J. Jeener, B.H. Meier, and R.R. Ernst, *J. Chem. Phys.* **71**, 4546 (1979).

[65]B.H. Meier and R.R. Ernst, *J. Am. Chem. Soc.* **101**, 6641 (1979).

[66]S. Macura and R.R. Ernst, *Mol. Phys.* **41**, 95 (1980).

[67]Anil Kumar, R.R. Ernst, and K. Wüthrich, *Biochem. Biophys. Res. Commun.* **95**, 1 (1980).

[68]M.P. Williamson, T.F. Havel, and K. Wüthrich, *J. Mol. Biol.* **182**, 295 (1985).

[69]A.D. Kline, W. Braun, and K. Wuthrich, *J. Mol. Biol.* **189**, 377 (1986).

[70]B.A. Messerle, A. Schäffer, M. Vasák, J.H.R. Kägi, and K. Wüthrich, *J. Mol. Biol.* **214**, 765 (1990).

[71]G. Otting, Y.Q. Qian, M. Billeter, M. Müller, M. Affolter, W.J. Gehring, and K. Wuthrich, *EMBO J.* **9**, 3085 (1990).

[72]T.F. Haveland and K. Wüthrich, *Bull. Math. Biol.* **46**, 673 (1984).

[73]W. Braun and N. Gō, *J. Mol. Biol. 186*, 611 (1985).

[74]R. Kaptein, E.R.P. Zuiderweg, R.M. Scheek, R. Boelens, and W.F. van Gunsteren, *J. Mol. Biol.* **182**, 179 (1985).

[75]G.M. Clore, A.M. Gronenborn, A.T. Brünger, and M. Karplus, *J. Mol. Biol.* **186**, 435 (1985).

[76]Y. Huang, S. Macura, and R.R. Ernst, *J. Am. Chem. Soc.* **103**, 5327 (1981).

[77]G.W. Eich, G. Bodenhausen, and R.R. Ernst, *J. Am. Chem. Soc.* **104**, 3731 (1982).

[78]P.H. Bolton and G. Bodenhausen, *Chem. Phys. Lett.* **89**, 139 (1982).

[79]The spectra were recorded by C. Griesinger, see R.R. Ernst, *Chimia* **41**, 323 (1987).

[80]L. Braunschweiler and R.R. Ernst, *J. Magn. Reson.* **53**, 521 (1983).

[81]D.G. Davis and A. Bax, *J. Am. Chem. Soc.* **107**, 2821 (1985).

[82]A.A. Bothner-By, R.L. Stephens, J. Lee, C.O. Warren, and R.W. Jeanloz, *J. Am. Chem. Soc.* **106**, 811 (1984).

[83]R. Brüschweiler, B. Roux, M. Blackledge, C. Griesinger, M. Karplus, and R.R. Ernst, *J. Am. Chem. Soc.* **114**, 2289 (1992).

[84]C. Griesinger, G. Otting, K. Wüthrich, and R.R. Ernst, *J. Am. Chem. Soc.* **110**, 7870 (1988).

[85]J. Briand and R.R. Ernst, *Chem. Phys. Lett.* **185**, 276 (1991).

[86]S. Vega, T.W. Shattuck, and A. Pines, *Phys. Rev. Lett.* **37**, 43 (1976).

[87]S. Vega and A. Pines, *J. Chem. Phys.* **66**, 5624 (1977).

[88]A. Wokaun and R.R. Ernst, *Mol. Phys.* **36**, 317 (1978).

[89]L. Braunschweiler, G. Bodenhausen, and R.R. Ernst, *Mol. Phys.* **48**, 535 (1983).

[90]A. Bax, R. Freeman, and S.P. Kempsell, *J. Am. Chem. Soc.* **102**, 4849 (1980).

[91]A. Bax, R. Freeman, and S.P. Kempsell, *J. Magn. Reson.* **41**, 349 (1980).

[92]U. Piantini, O.W. Sørensen, and R.R. Ernst, *J. Am. Chem. Soc.* **104**, 6800 (1982).

[93]N. Müller, G. Bodenhausen, K. Wüthrich, and R.R. Ernst, *J. Magn. Reson.* **65**, 531 (1985).

[94]C. Radloff and R.R. Ernst, *Mol. Phys.* **66**, 161 (1989).

[95]A. Wokaun and R.R. Ernst, *Chem. Phys. Lett.* **52**, 407 (1977).

[96]G. Bodenhausen, H. Kogler, and R.R. Ernst, *J. Magn. Reson.* **58**, 370 (1984).

[97]M.H. Levitt and R.R. Ernst, *Chem. Phys. Lett.* **100**, 119 (1983).

[98]M.H. Levitt and R.R. Ernst, *J. Chem. Phys.* **83**, 3297 (1985).

[99]C. Griesinger, O.W. Sørensen, and R.R. Ernst, *J. Am. Chem. Soc.* **107**, 6394 (1985).

[100]C. Griesinger, O.W. Sørensen, and R.R. Ernst, *J. Chem. Phys.* **85**, 6837 (1986).

[101]C. Griesinger, O.W. Sørensen, and R.R. Ernst, *J. Magn. Reson.* **75**, 474 (1987).

[102]A. Bax and R. Freeman, *J. Magn. Reson.* **44**, 542 (1981).

[103]B.U. Meier and R.R. Ernst, *J. Magn. Reson.* **79**, 540 (1988).

[104]A.A. Maudsley and R.R. Ernst, *Chem. Phys. Lett.* **50**, 368 (1977).

[105]G. Bodenhausen and R. Freeman, *J. Magn. Reson.* **28**, 471 (1977).

[106]L. Müller, *J. Am. Chem. Soc.* **101**, 4481 (1979).

[107]M. Ernst, C. Griesinger, R.R. Ernst, and W. Bermel, *Mol. Phys.* **74**, 219 (1991).

[108]M.H. Levitt, O.W. Sørensen, and R.R. Ernst, *Chem. Phys. Lett.* **94**, 540 (1983).

[109]H. Kogler, O.W. Sørensen, G. Bodenhausen, and R.R. Ernst, *J. Magn. Reson.* **55**, 157 (1983).

[110]H.D. Plant, T.H. Mareci, M.D. Cockman, and W.S. Brey, *27th Experimental NMR Conference* (Baltimore, MA, USA) 1986.

[111]G.W. Vuister and R. Boelens, *J. Magn. Reson.* **73**, 328 (1987).

[112]C. Griesinger, O.W. Sørensen, and R.R. Ernst, *J. Magn. Reson.* **73**, 574 (1987).

[113]C. Griesinger, O.W. Sørensen, and R.R. Ernst, *J. Am. Chem. Soc.* **109**, 7227 (1987).

[114]H. Oschkinat, C. Griesinger, P. Kraulis, O.W. Sørensen, R.R. Ernst, A.M. Gronenborn, and G.M. Clore, *Nature (London)* **332**, 374 (1988).

[115]G.W. Vuister, R. Boelens, and R. Kaptein, *J. Magn. Reson.* **80**, 176 (1988).

[116]C. Griesinger, O.W. Sørensen, and R.R. Ernst, *J. Magn. Reson.* **84**, 14 (1989).

[117]E.R.P. Zuiderweg and S.W. Fesik, *Biochemistry* **28**, 2387 (1989).

[118]D. Marion, P.C. Driscoll, L.E. Kay, P.T. Wingfield, A. Bax, A.M. Gronenborn, and G.M. Clore, *Biochemistry* **28**, 6150 (1989).

[119]S. Boentges, B.U. Meier, C. Griesinger, and R.R. Ernst, *J. Magn. Reson.* **85**, 337 (1989).

[120]O.W. Sørensen, *J. Magn. Reson.* **89**, 210 (1990).

[121]L.E. Kay, G.M. Clore, A. Bax, and A.M. Gronenborn, *Science* **249**, 411 (1990).

[122]Z.L. Mádi, C. Griesinger, and R.R. Ernst, *J. Am. Chem. Soc.* **112**, 2908 (1990).

[123]R. Brüschweiler, M. Blackledge, and R.R. Ernst, *J. Biomol. NMR* **1**, 3 (1991).

[124]W. Burgermeister, T. Wieland, and R. Winkler, *Eur. J. Biochem.* **44**, 311 (1974).

[125]H. Kessler, M. Klein, A. Müller, K. Wagner, J.W. Bats, K. Ziegler, and M. Frimmer, *Angew. Chem.* **98**, 1030 (1986); *Angew. Chem. Int. Ed. Engl.* **25**, 997 (1986); H. Kessler, A. Müller, and K.H. Pook, *Liebigs Ann. Chem.*, 903 (1989); H. Kessler, J.W. Bats, J. Lautz, and A. Müller, *Liebigs Ann. Chem.*, 913 (1989); J. Lautz, H. Kessler, W.F. van Gunsteren, H.J. Berendsen, R.M. Scheek, R. Kaptein, and J. Blaney, *Proc. 20th Eur. Pept. Symp.*, (Eds.: G. Jung, E. Bayer), 438 (1989).

[126]R.R. Ernst, M. Blackledge, S. Boentges, J. Briand, R. Brüschweiler, M. Ernst, C. Griesinger, Z.L. Mádi, T. Schulte-Herbrüggen, and O.W. Sørensen, in "Proteins, Structure, Dynamics, Design" (Eds.: V. Renugopalakrishnan, P.R. Carey, I.C.P. Smith, S.G. Huang, and A.C. Storer), ESCOM, Leiden, 1991.

[127]P.C. Lauterbur, *Nature* **242**, 190 (1973).

[128]Anil Kumar, D. Welti, and R.R. Ernst, *J. Magn. Reson.* **18**, 69 (1975).

[129]W.A. Edelstein, J.M.S. Hutchison, G. Johnson, and T.W. Redpath, *Phys. Med. Biol.* **25**, 751 (1980).

[130]P. Mansfield, A.A. Maudsley, and T. Baines, *J. Phys.* **E9**, 271 (1976).

[131]P.C. Lauterbur, D.M. Kramer, W.V. House, and C.-N. Chen, *J. Am. Chem. Soc.* **97**, 6866 (1975).